

# Thermal Characterization of MBBA, 5CB, and 8CB for Thermal Switches Using the $3\omega$ Method

Bolesław L. Osiński

Advisor: Kevin J. Malloy

Undergraduate Honors Thesis  
University of New Mexico  
Department of Physics and Astronomy  
April 18, 2011

## **Abstract**

Liquid crystals can be used in thin film heat switches for micro-electronics thermal management. We present the first electrically controllable liquid crystal thin film heat switch that can thermally characterize itself with a metal line which simultaneously heats the thin films, measures their thermal characteristics, and acts as an electrode. The thermal conductivities of three liquid crystal thin films (MBBA, 5CB, and 8CB) are measured as a function of temperature and alignment voltage using the  $3\omega$  technique. The results allow us to infer critical phase transition temperatures, switching voltages, and alignments of the liquid crystal molecules.

# Contents

Abstract .....	2
Introduction .....	5
1 Fundamental Properties of Liquid Crystals	5
1.1 Liquid Crystal Phases .....	5
1.2 Order Parameter .....	6
1.3 Some Background on MBBA, 5CB, and 8CB .....	7
1.4 Alignment in Magnetic Fields .....	8
1.5 Alignment in Electric Fields .....	9
2 The $3\omega$ Technique	10
2.1 Origin of The $3\omega$ Signal .....	10
2.2 Solution of the Heat Equation for Thin Line Geometry .....	11
3 Instrumentation	13
3.1 SR830 Lock-In Amplifier .....	13
3.2 Lake Shore 330 Temperature Controller .....	13
3.3 Keithley 2010 Multimeter .....	14
3.4 Keithley 617 Programmable Electrometer .....	14
4 Heater Fabrication	14
4.1 Mask Design .....	14
4.2 Photolithography .....	15
4.3 Metal Evaporation .....	16
5 Sample Preparation	17
6 Experimental Considerations	18
6.1 $3\omega$ Noise Floor .....	18
6.2 Determination of Frequency Range .....	20

6.3	Staying in the Linear I-V Regime .....	22
6.4	Heater Defects .....	22
7	Experimental Procedure .....	24
7.1	Preliminary Tests .....	24
7.2	Measurements of $\kappa$ vs. T .....	25
7.3	Measurements of $\kappa$ vs. V .....	26
8	Results and Discussion .....	26
8.1	Temperature Dependence of Thermal Conductivity .....	26
8.1.1	Glass .....	26
8.1.2	MBBA .....	27
8.1.3	5CB .....	29
8.1.4	8CB .....	30
8.2	Measurements of Thermal Conductivity Anisotropy .....	31
8.2.1	Glass .....	31
8.2.2	MBBA .....	32
8.2.3	5CB .....	33
8.2.4	8CB .....	34
8.3	A persistent Factor of 2 .....	35
8.3.1	Comparison with Numerical Solution .....	36
8.3.2	Factor of 2 as a Calibration Factor .....	37
9	Conclusion .....	38
	References .....	39
	Appendix .....	41
A.	LabVIEW Instrument Control Code .....	41
B.	MATLAB Data Analysis Code .....	42

# Introduction

The applications of thin film technology are ever expanding. Among these are novel approaches to thermal management. An electrically controllable thin film heat engine could manage thermal transport in micro-electronics and across large surface areas alike without the use of bulky fans. This idea has been discussed in a recent paper by Epstein and Malloy [1]. Their model consists of an electrocaloric thin film material sandwiched between two thin film heat switches. Theoretical calculations suggest that such a thin film heat engine could achieve efficiencies of over 60 % of the Carnot cycle, which is significantly higher than most commercial vapor compression devices. The heat switches on either side of the electrocaloric thin film must be made out of a material whose thermal conductivity can be electrically switched. Because of their anisotropic geometry, liquid crystals exhibit anisotropic thermal conductivity and are potential candidates for a thin film heat switch. This thesis focuses on measuring the temperature dependence and anisotropy of the thermal conductivity ( $\kappa$ ) of three well known liquid crystals (MBBA, 5CB, 8CB). We measure  $\kappa$  with a non-adiabatic technique known as the  $3\omega$  technique, which is described in detail in the paper. This technique is particularly convenient for measuring thermal properties of heat switches as the heating element itself can be used as an electrode for electric field application. To our knowledge, our research is the first to employ the heater-thermometer used for the  $3\omega$  method as an electrode.

## 1. Fundamental Properties of Liquid Crystals

Liquid crystals (LCs) are molecular fluids composed of rod-like molecules that exhibit several distinct mesophases between entirely solid and liquid phases. When the first mathematical descriptions of anisotropic fluids were developed by Onsager in the 1940s, LCs were only studied as an extension of fluid dynamics by a few curious scientists. Since then an enormous body of interdisciplinary research has accumulated on the subject, making LC research a field of its own. We begin by acquainting the reader with some of the most essential characteristics of liquid crystals before describing the experiments. The information for this section is taken largely from the two most referenced texts on LCs [2][3], which may be consulted should the reader desire greater detail.

### 1.1 Liquid Crystal Phases

The three primary liquid crystal mesophases, known as smectic, cholesteric, and nematic phases, are characterized by unique long range alignments. Discussion of cholesteric phases is omitted here as the LCs chosen for this research exhibit only smectic and nematic phases. Smectic phases, of which there are many, are characterized by stratified structures with various possible molecular arrangements within each stratification. Two common smectic phases are depicted in Fig. 1. In the smectic A phase individual molecules are oriented perpendicular to the

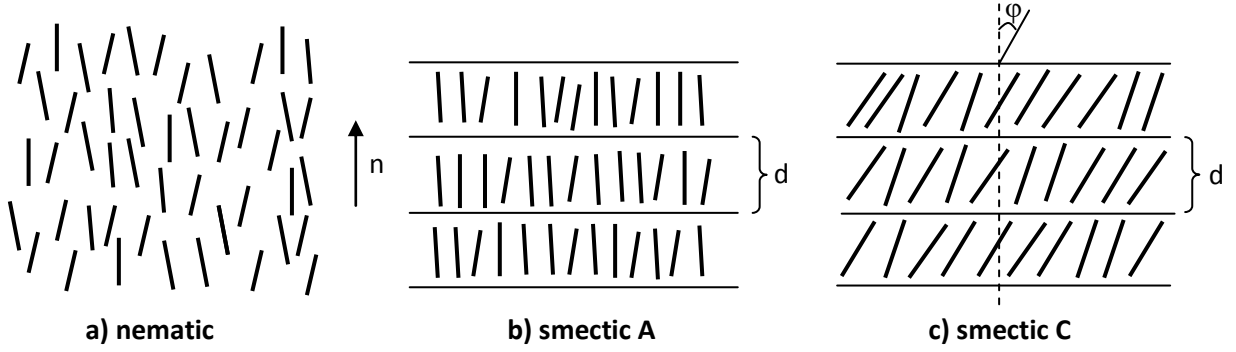


**FIG.1** a) The nematic phase possesses orientational order but lacks positional order. The individual molecular axes point along an average direction,  $\mathbf{n}$ , known as the director. b) In the smectic A phase molecules assume stratified arrangements but each layer behaves as a two-dimensional liquid with axes perpendicular to the layer boundary. c) Closely related to the smectic A phase, the smectic C phase has molecules oriented at an angle  $\phi$  to the layer boundary.

boundary between layers while in the smectic C phase individual molecules are aligned at an angle to the boundary. The smectic B phase exhibits the same axis orientation as the smectic A phase, but the molecules within each layer are further ordered in a hexagonal lattice. The only LC we use exhibiting a smectic phase is 8CB. The spacing of adjacent layers in the 8CB smectic A phase is significantly longer than the length of the molecule, indicating anti-parallel arrangements in which benzene rings fit alongside hydrocarbon tails (see Fig. 3 below for a visualization of the molecular structure).

Some LCs may transition between numerous smectic phases within a narrow temperature range. However, above a critical temperature,  $T_{SmN}$ , liquid crystals will transition to the nematic phase. In the nematic phase, also depicted in Fig. 1, the centers of gravity of the molecules have no long range order, but the orientations of their long axes exhibit long range directional order. Above yet another critical temperature,  $T_{NI}$ , LCs undergo a phase transition to a conventional (isotropic) liquid phase. The nematic phase is not characterized by any particular director angle with respect to the bounding surface containing the LC. Depending on the surface treatment, the nematic phase LCs may align parallel (homogeneous alignment), perpendicular (homeotropic alignment), or at an intermediate angle to the surface.

## 1.2 Order Parameter

The degree of alignment of a liquid crystal in the nematic phase (or within a stratification of a smectic phase) is characterized by an order parameter

$$S = \langle P_2(\cos\theta) \rangle = \frac{1}{2} \langle 3\cos^2\theta - 1 \rangle = \int f(\theta) \frac{1}{2} (3\cos^2\theta - 1) d\Omega \quad (1)$$

where  $P_2(\cos\theta)$  is the second order Legendre polynomial,  $\theta$  is the angle between the director  $\mathbf{n}$  (the average direction of alignment) and the direction of a given molecule, and  $f(\theta)$  is the



synthesized and the cyanobiphenyls became the first viable liquid crystals for commercialization in the UK liquid crystal industry. Over the decades to come the TN mode (described in detail in [9]) has become one of the dominant operational modes for modern LCDs. The cyanobiphenyls not only have the positive  $\Delta\epsilon$  necessary for TN mode operation but also contain a highly polar CN head group that greatly enhances alignment with electric fields and allows for much lower operational voltages. The molecular structures and approximate phase transition temperatures of the three LCs are presented in Fig. 3.

## 1.4 Alignment in Magnetic Fields

Many organic molecules are diamagnetic, particularly when they are aromatic (possessing a benzene ring). The LCs whose thermal properties are measured possess (two) benzene rings each. When a benzene ring is exposed to a changing magnetic field  $\mathbf{H}$ , a current builds which tends to reduce the magnetic flux of the component of  $\mathbf{H}$  along the normal to the plane of the ring according to Lenz's law. Thus a benzene molecule tends to choose an orientation such that  $\mathbf{H}$  is in the plane of the ring. This effect is quite low in magnitude for a single molecule and is hardly strong enough to overcome the thermal motion. But if we take numerous molecules the alignment effect is quite noticeable. Because of competition between thermal motion, surface orientation forces, and field orientation LCs will not show any alignment for arbitrarily small field strengths, but will begin to align only above a critical field strength

$$H_{c,i} = \left(\frac{\pi}{d}\right) \left(\frac{K_i}{\Delta\chi}\right)^{1/2} \quad (2)$$

where  $i$  runs from 1 to 3 indicating splay, twist, and bend elastic constants and  $\Delta\chi = \chi_{\parallel} - \chi_{\perp}$  is

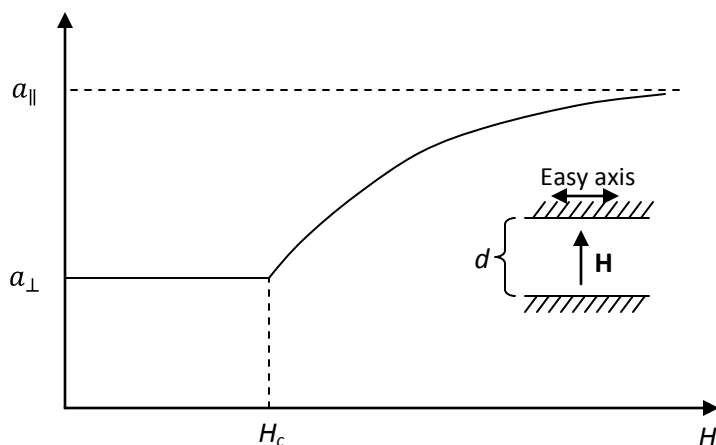


**Fig 4.** An inset shows arrangement of an experiment for detecting the Freedericksz transition. The LC thin film has thickness  $d$ .  $\mathbf{H}$  points along surface normal while the easy axis for LC alignment is along the surface. For  $H < H_c$  equilibrium thermodynamics dominates and the LCs are parallel to the surface (perpendicular to the field). Thus we measure the component of the generic anisotropic property,  $a$ , perpendicular to the molecular axis ( $a_{\perp}$ ). As  $H$  increases beyond  $H_c$  the LCs align perpendicular to the surface (along the field) and measurements saturate at the component of  $a$  along the molecular axis ( $a_{\parallel}$ ).

the anisotropic magnetic susceptibility. Such a transition was first studied by Fredericksz in 1927 by optical methods and now bears his name. He found that  $H_c$  is inversely proportional to the cell thickness  $d$ ,  $H_c d = \text{const}$ . This transition can be detected by measuring any anisotropic property, such as dielectric constant or thermal conductivity, as field strength increases. Fig. 4 is a plot showing the typical onset of a Fredericksz transition in a measurement of a generic anisotropic property,  $a$ .

## 1.5 Alignment in Electric Fields

Most LC technologies use electric fields rather than magnetic fields for alignment. For low field strengths the behavior of LCs in magnetic and electric fields are analogous. The critical electric field  $E_c$  is related to the critical magnetic field though the substitution  $\frac{1}{2}\Delta\chi H^2 \rightarrow \frac{\Delta\epsilon E^2}{8\pi}$ , giving

$$E_c = \left( \frac{4\pi\Delta\chi}{\Delta\epsilon} \right)^{1/2} H_c \quad (3)$$

where  $\Delta\epsilon = \epsilon_{\parallel} - \epsilon_{\perp}$  is the dielectric anisotropy. At higher field strengths, however, the behavior of organic LCs in electric fields is markedly more complex than in magnetic fields because the coupling of an external electric field to a nematic medium involves the inherent anisotropy of the dielectric constant, induced electric dipoles, and dipole orientations. Alignment with magnetic fields, on the other hand, is well described by only considering the torque applied to an induced magnetic dipole. Almost all liquid crystals have positive magnetic susceptibilities ( $\Delta\chi > 0$ ), but their dielectric anisotropies vary greatly. This gives rise to a great diversity of responses to electric fields. As described above, MBBA has negative  $\Delta\epsilon$  while cyanobiphenyls have positive  $\Delta\epsilon$ . In order to minimize the electrical energy [8]

$$f_e = -\frac{1}{2}\epsilon_{\perp}\epsilon_o E^2 - \frac{1}{2}\Delta\epsilon\epsilon_o(\mathbf{n} \cdot \mathbf{E})^2 \quad (4)$$

LCs with positive  $\Delta\epsilon$  will align with major axes along the field while those with negative  $\Delta\epsilon$  will align with major axis perpendicular to the field.

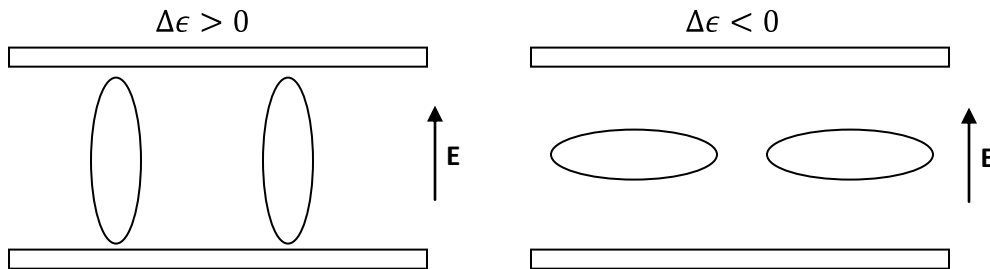


**FIG. 5** LCs with positive  $\Delta\epsilon$  will align with major axis along  $\mathbf{E}$  while LCs with negative  $\Delta\epsilon$  will align with major axis perpendicular to  $\mathbf{E}$ .

## 2. The $3\omega$ Technique

Typical thermal measurements that rely on a temperature gradient across a thin film created by a steady heat flow usually encounter problems due to radiative heat loss when performed near room temperature. Quasiadiabatic AC measurements largely overcome these radiative errors, but for materials, such as organic liquids, with low thermal diffusivities these measurements are restricted to low heat oscillation frequencies because the heat wave must be allowed enough time to reach the other side of the thin film [12]. We adapt a non-adiabatic AC technique, known as the  $3\omega$  method, which drops the restriction on low heat oscillation frequency by using the heating element simultaneously as a thermometer.

Developed by Cahill [10] for a thin line heater geometry, the  $3\omega$  method differs from most other thermal measurement techniques by measuring the frequency ( $\omega = 2\pi f$ ) dependence of temperature oscillations instead of the time-domain response. An AC voltage at frequency  $\omega$  is applied across a thin metal line. This leads to a resistance oscillation of the line at  $2\omega$  due to Joule heating. Mixing of the  $2\omega$  resistance oscillation and the driving current at  $\omega$  produces a small voltage at  $3\omega$  across the line that contains thermal information of the sample. Thus the line acts as both a heater and a thermometer. The  $3\omega$  method allows one to measure the thermal properties of thin films and bulk materials alike. It is particularly well suited for measuring thermal properties of liquids as the low heat fluxes produce minimal convection effects. The characteristic length of the thermal wave generated by the metal line, which scales as  $1/(\omega^{1/2})$ , is in principle limited only by the requirement that it be shorter than the thickness of the thin film. In practice, however, it must also be much longer than the thickness of the metal line so as to ensure that the thin film properties, and not those of the metal line itself, are being measured.

### 2.1 Origin of the $3\omega$ Signal

An AC current of frequency  $\omega$  passing through a metal heater will cause Joule heating at  $2\omega$ . Due to the non-zero temperature coefficient,  $\alpha \equiv (1/R)(dR/dT)$ , of the metal, the resistance of the heater also oscillates at  $2\omega$  according to

$$R(t) = R_o[1 + \alpha|\Delta T| \cos(2\omega t + \varphi)] \quad (5)$$

where the amplitude of the temperature oscillations in the heater  $\Delta T$  is generally complex and is shifted by a phase  $\varphi$  from the power oscillation. The voltage across the heater is therefore

$$\begin{aligned} V(t) &= I(t)R(t) = I_o \cos(\omega t) * R_o[1 + \alpha|\Delta T| \cos(2\omega t + \varphi)] \\ &= I_o R_o \cos(\omega t) + \frac{1}{2} I_o R_o \alpha |\Delta T| \cos(\omega t + \varphi) + \frac{1}{2} I_o R_o \alpha |\Delta T| \cos(3\omega t + \varphi) \end{aligned} \quad (6)$$

where the identity  $\cos(a * b) = (1/2) [\cos(a + b) + \cos(a - b)]$  has been used to explicitly show the dependence on  $3\omega$  in the third term. Both the second and third terms include  $|\Delta T|$ , but

because the second term oscillates at  $\omega$  it cannot be easily resolved from the much larger first term. In order to extract the thermal information from the third term a lock-in amplifier is used to measure the  $3\omega$  signal.

## 2.2 Solution of the Heat Equation for Thin Line Geometry

A thin line heater of length  $l$  can be treated as a superposition of many infinitely narrow lines over its width,  $2b$ , as shown in Fig. 6.

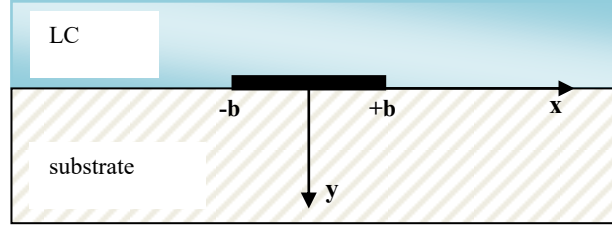


**FIG. 6.** A side view of the heater and the sample. The heater is modeled as a superposition of infinitely thin lines from  $x = -b$  to  $x = b$  and is much thinner than the sample so that it has negligible effect on the temperature profile of the sample.

The solution to the heat equation for an infinitely narrow line on the surface of a solid substrate can be found in Carslaw and Jaeger [11]

$$\Delta T(r) = \left( \frac{P}{\pi l \kappa} \right) K_0(qr) \quad (7)$$

where  $r^2 = x^2 + y^2$  is the radial coordinate perpendicular to the line,  $P/l$  is the power per unit length generated in the metal line, and  $K_0$  is the zeroth-order modified Bessel function. The quantity  $q$  is the complex thermal wave number

$$q = \sqrt{\frac{i2\omega C_p}{\kappa}} \quad (8)$$

The characteristic length of the exponentially decaying thermal oscillation, which we call the thermal penetration depth, is given by  $\lambda = |1/q|$  and should be shorter than the thickness of the sample to avoid interference from the upper boundary of the sample. One should note that  $C_p$  must be the volumetric specific heat capacity at constant pressure with units ( $\text{kJ}/\text{m}^3\text{-K}$ ) so that  $\lambda$  has units of meters.

We are interested in the heat oscillation at the surface of the heater and so we set  $y = 0$ . Cahill [10] takes the Fourier transform of Eq. (7), explaining that it conveniently allows one to include the finite width,  $2b$ , of the heater by multiplying the transformed equation by the Fourier

transform of the heat source. Assuming that heat enters the sample evenly over the width of the line he finds the average temperature oscillation at the surface of the heater to be

$$\Delta T = \frac{P}{\pi l \kappa} \int_0^\infty \frac{\sin^2(kb)}{(kb)^2 (k^2 + q^2)^{1/2}} dk \quad (9)$$

where  $k$  is the Fourier space variable. Fig. 7 is a numerical evaluation of Eq. (9) for realistic values of  $\kappa$  and  $C_p$  for glass. Although an analytic expression to Eq. (9) is not known, we can set

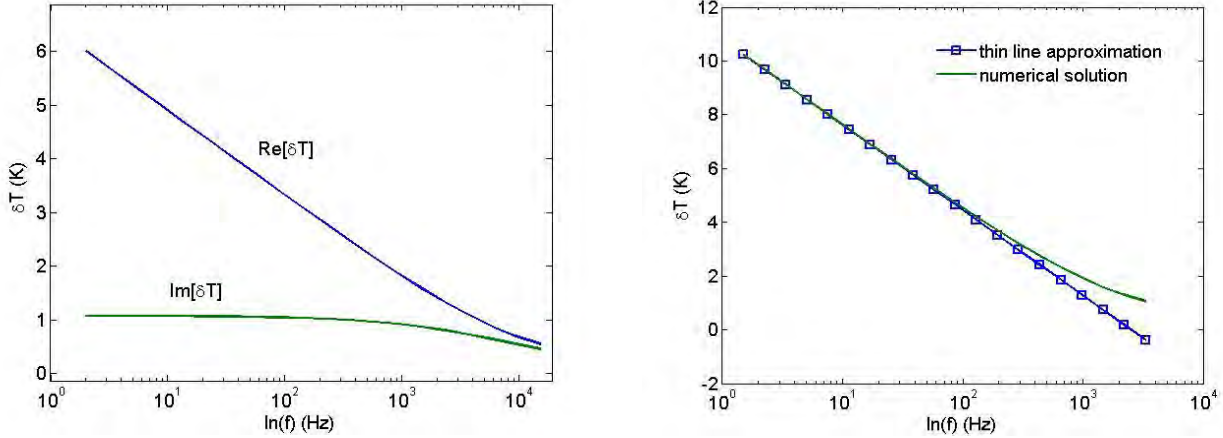


**FIG. 7** Left: Numerical evaluation of Eq. (9) for a 10  $\mu\text{m}$  wide heater with resistance  $R = 30 \Omega$  on a glass substrate with  $\kappa = 1.1 \text{ W/m}\cdot\text{K}$  and  $C_p = 2200 \text{ kJ/m}^3\cdot\text{K}$  (typical values for glass). Right: At high frequencies  $\text{Re}[\Delta T]$  and  $\ln(f)$  cease to be linearly related because  $\lambda$  has entered the planar regime with respect to  $b$ . Therefore plots of the real part of the numerical solution (Eq. (9)) and the thin line approximation (Eq. (10)) diverge from each other at high frequencies.

$\sin(kb)/(kb) = 1$  to simplify the integration in the limit that  $\lambda \gg b$ . The result of the integration is

$$\Delta T = \frac{P}{2\pi l \kappa} \left( -\ln\left(\frac{i2\omega b^2 C_p}{\kappa}\right) + 0.922 \dots \right) = -\frac{P}{2\pi l \kappa} \ln(\omega) + \text{const} \quad (10)$$

From this we can see that as long as  $\lambda \gg b$  the thermal conductivity,  $\kappa$ , can be determined from the slope of the real part  $\text{Re}[\Delta T]$  as a function of  $\ln(\omega)$ . However, when the thermal penetration depth is shorter than the heater width ( $\lambda \ll b$ ), the heat no longer flows radially outward as from a thin line, but along the heater surface normal as from a flat plane and this approximation diverges from the solution. The  $3\omega$  technique was first applied to this planar heating regime by Birge and Nagel [12], who showed that this configuration allows measurement of the product of thermal conductivity and specific heat ( $\kappa C_p$ ). Originally, I had hoped to make measurements in both regimes, but measurements in the thin line regime presented sufficiently many problems so as to occupy the entire time allotted for this project.

So far we have only described heat diffusion through one side of the heater, so we must generalize the solutions to represent heat diffusion through both sides of the heater. For the case of a thin line heater one may neglect the thermal boundary mismatch between the substrate and sample if the thermal penetration depths do not substantially differ. In the case of an organic liquid, with a thermal diffusivity [10] typically near  $10^{-7}$  m<sup>2</sup>/s, on a soda-lime glass substrate, with a thermal diffusivity near  $3.5 \times 10^{-7}$  m<sup>2</sup>/s, the thermal penetration depths differ by 76%, making this a rather crude approximation. Neglecting the mismatch, however, has the convenient consequence that the measured thermal conductivity is just the sum of the thermal conductivities of the substrate and liquid sample [13][14]. Solving for  $\kappa$  in the first term of Eq. (10) we can write an expression for the total thermal conductivity of the liquid/substrate system

$$\kappa_s + \kappa_l = -\frac{P}{2\pi l} * \frac{d\ln(f)}{d\text{Re}[\Delta T]} \quad (11)$$

where the subscript  $s$  stands for substrate,  $l$  stands for liquid, and the term furthest to the right is simply the reciprocal of the slope of  $\text{Re}[\Delta T]$  as a function of  $\ln(f)$ .

## 3. Instrumentation

### 3.1 SR830 Lock-in Amplifier

The lock-in amplifier powers the heater and measures the AC voltage across the heater. Because the SR830 has built in frequency multipliers and a dynamic reserve greater than 100 dB there is no need for a Wheatstone bridge to filter out the signal at  $\omega$  as was done in previous papers[10][12][13]. The lock-in also possesses a built in AC voltage source with an output range of 0.004 V to 5.0 V. It is important to note that the maximum output of 5.0 V is only achievable for loads whose resistance is greater than the 50  $\Omega$  output impedance of the lock-in [15]. Therefore, If a heater resistance is too low then the lock-in will not be able to deliver enough power to generate a  $3\omega$  signal that is well above the  $3\omega$  noise floor inherent in the instrument (see section 6.1). The time constant of the lock-in is set to 1s second for low frequency measurements (below 1 kHz) and to 1ms for high frequency measurements (above 1 kHz). Synchronous filtering is applied automatically by the lock-in for frequencies below 200 Hz. The lock-in is used in a standard 4 point measurement configuration to measure both the first and third harmonics of the voltage across the heater.

### 3.2 Lake Shore 330 Temperature Controller

The temperature controller uses a calibrated Si diode to measure temperature changes within a resolution of 0.1 K. Four phosphor bronze 36 AWG wires coated with polyimide insulation make contact with the temperature controller in a standard 4 point configuration to

measure the resistance of the Si diode sensor. The temperature controller is designed to work with either a 25  $\Omega$  or a 50  $\Omega$  heater. We choose to use a 25  $\Omega$  silicone-encased flat heater manufactured by Hi-Heat Industries Inc. to heat the copper stage. The temperature controller uses P, I, and D parameters to algorithmically determine the heat output needed to reach a certain temperature [16]. P and I parameters are systematically determined by observing the speed at which the desired temperature is reached as they are adjusted. D is set to 0.

### **3.3 Keithely 2010 Multimeter**

Calculation of the thermal properties of the sample requires knowledge of the temperature coefficient of resistance of the heater. In general the temperature coefficient of a thin film of a metal is not identical to its bulk value and so we must measure it ourselves. The 2010 Multimeter measures the voltage across a 5  $\Omega$  precision resistor in series with the heater, thus giving the current through the heater. The resistance can then be calculated because the voltage across the heater is constantly monitored by the lock-in. The 2010's measurement accuracy is affected by the crest factor of the waveform (the ratio of the peak value to the RMS value). The maximum fundamental frequency at which the corresponding crest factor must be taken into account is 500 Hz [17], therefore all measurements with the multimeter are made with lock-in output voltages at 1kHz, well above 500 Hz.

### **3.4 Keithley 617 Programmable Electrometer**

This instrument is used solely for its DC voltage source, which ranges from -100 V to 100 V. The heater itself is connected to the negative output of the Keithley 617, acting as a negative electrode. Measurements of  $V_{1\omega}$  and  $V_{3\omega}$  on an empty cell with and without applied DC voltage agree within experimental error so we may assume that the DC electric field applied perpendicular to the heater by the 617 is decoupled from the AC field which powers the heater.

## **4. Heater Fabrication**

### **4.1 Mask Design**

Heaters are produced by evaporating metals through a mask patterned by photolithography onto a glass substrate. In order to produce the desired  $3\omega$  signal, the heaters must be much thinner than they are long. Previous papers reported thin line heaters from 5  $\mu\text{m}$  to 80  $\mu\text{m}$  with lengths of approximately 1 cm and thicknesses between 100 and 300 nm. After two prototype designs, our final design for the photolithography mask, shown in Fig. 8, consists of three thin line patterns (of widths 10, 20, 40  $\mu\text{m}$ ) and two planar patterns (of widths 1.5 and 3 mm). Patterns for the top electrodes were designed so as to fit directly over the heaters, with large contact pads for electrical contact. The patterns were designed using the free software Layout Editor<sup>TM</sup> and were manufactured by FineLine Imaging Inc. The mask was designed with

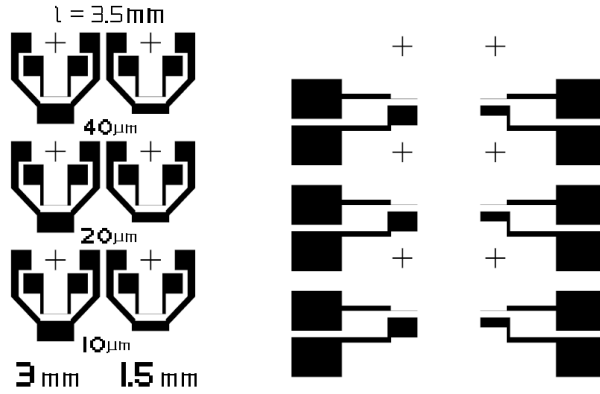


**FIG. 8** Left: Three thin line heaters with widths of 10, 20, and 40  $\mu\text{m}$  are paired with two planar heaters with widths of 1.5 and 3 mm. Right: The mask pattern for the top electrodes fits right over the heater mask. The small crosses are used for alignment of the two patterns.

both thin line and planar heater geometries in close proximity so as to measure a single heater in both heat flow regimes. However, this arrangement proved to be too ambitious for the time allotted, as measurements in the thin line regime alone provided sufficiently many difficulties to overcome.

The legs of the thin line heater must be much wider than the line itself so that heat is dissipated primarily in the line and the voltage measured across the heater is close to that across the line itself. The thin film sample partly covers the legs, so the entire  $3\omega$  signal does not come from the thin line alone. Using the resistivity of Au ( $22.14 \text{ n}\Omega\cdot\text{m}$ ) the resistance of a 20  $\mu\text{m}$  wide line is  $12.915 \Omega$ , while the resistance of a 500  $\mu\text{m}$  wide leg is only  $0.4428 \Omega$  (assuming their lengths are equal). Applying 1 V across the heater dissipates 2.3 mW of power across a leg and 67.8 mW across the line, so we can be sure that most of the heating occurs at the line.

## 4.2 Photolithography

It is important to develop a photolithography procedure that makes reproducible high quality samples. Generally, photolithography procedures begin with spinning a thin layer of photo-active chemical (called photoresist) onto the surface of the sample. The chemical is then dried by placing the sample on a hot plate or in an oven. Once hardened, the photoresist is exposed to UV light through a mask. Unlike most masks, our mask is not a reverse image (it is the pattern itself), and therefore image reversing (IR) photoresist must be used. The thinness of the heater lines requires the resolution to be about  $1 \mu\text{m}$  for good results. We found that backscattering of UV light off of the metal surface of the sample chuck would over expose the regions of interest. Because the thickness of the glass slides is much greater than thickness of the line, light need not reflect over a large angle to flood the line, leading to a complete removal of the metal heater during the liftoff process. A 2 inch square slice of black paper placed under the glass slide sufficed to absorb the UV light enough so that lines clearly developed. Below is the step-by-step procedure used to fabricate our heaters.

- Clean glass with soap, followed by IPA, acetone, and methanol
- Etch glass in 1:10 HF / H<sub>2</sub>O solution for 20 minutes
- Rinse in distilled water
- When dry apply HMDS adhesive and spin for 30 s at 5000 rpm
- Apply AZ 5214-IR photoresist and spin for 30 s at 5000 rpm
- Soft bake glass slide for 90 s at 90° C to ensure it does not stick to mask during exposure
- Expose for 3.5 s with constant intensity UV light (monitoring 365 nm)
- Hard bake glass slide for 60 s at 112°
- Flood expose to constant intensity UV light for 30 s to promote the polymer reaction
- Develop in 1:4 diluted AZ developer for 30 s
- O<sub>2</sub> plasma clean for 3 min at 50W
- Deposit 10 nm Ti followed by 300 nm Au

The etching step is included so as to improve metal-glass adhesion. However, etched surfaces tend to induce homeotropic alignment of liquid crystals (along the normal to the glass surface), which is undesirable for 5CB and 8CB (with positive  $\Delta\epsilon$ ) as they would already be aligned in the direction expected from an applied electric field (see section 1.5). Application of an electric field would therefore have no measurable orientation effect on the thermal conductivity. MBBA (with negative  $\Delta\epsilon$ ), on the other hand, will align along the surface with an applied electric field, and therefore a homeotropic initial alignment is desirable for measurable orientational effect.

### 4.3 Metal Evaporation

Once a photoresist mask is successfully created, metal is evaporated through the mask onto the glass substrate. The evaporation takes place in chamber that is cryogenically pumped down to pressures below  $2 \times 10^{-6}$  Torr. A high power electron beam is magnetically steered into a circular pattern that uniformly heats the metal contained by a small carbon crucible. After evaporation, the photoresist is removed by soaking in acetone. This process is known as liftoff. A pressurized acetone jet is used to remove flakes that do not come off on their own. The entire process, from pumping down to liftoff takes approximately 4 hours.

Originally, we chose to evaporate Ni because its relatively high resistance and temperature coefficient promised a good heater. However, most attempts to produce thin line Ni heater-thermometers were met with failure as the heaters would often peel off before they could be used. This persistent difficulty led us to forgo further use of Ni for thin line heaters. Because Ti is known to adhere well to smooth surfaces [19] we evaporate a 10 nm adhesion layer of Ti, followed by a 300 nm layer of Au, which is chosen primarily because it does not oxidize. The thickness of the heater layer is chosen so that the resistance of the heater is high enough that the maximum 5 V output of the lock-in can produce a  $3\omega$  signal on the order of 1 mV, which is well above the  $3\omega$  noise floor. In practice, thin line heaters with resistances in the range of 10 - 100  $\Omega$

give the best results. The resistance of the heater can in principle be quite high, but this would require very thin heater layers, which are easily damaged.

## 5. Sample Preparation

Newly fabricated heaters and top electrodes are cleaned with IPA and acetone, rinsed in DI water, and dried with high pressure  $N_2$ . Excess glass is cleaved from the top electrode substrate in order to allow access for probes to make contact with the heater contact pads. The heater and top electrode are unidirectionally rubbed to create micro-grooves that will align the LC molecules at the surface [20]. Two small strips of double sided scotch tape are then applied to either side of the thin line heater to act as spacers and to hold the sample cell together. Under a microscope each top electrode is carefully aligned by hand above the heater line and then pressed down to stick to the double-sided tape. Fig. 9 is a side view of a completed cell. Double-sided scotch tape was used primarily for its convenience as it allowed for quick sample preparation.

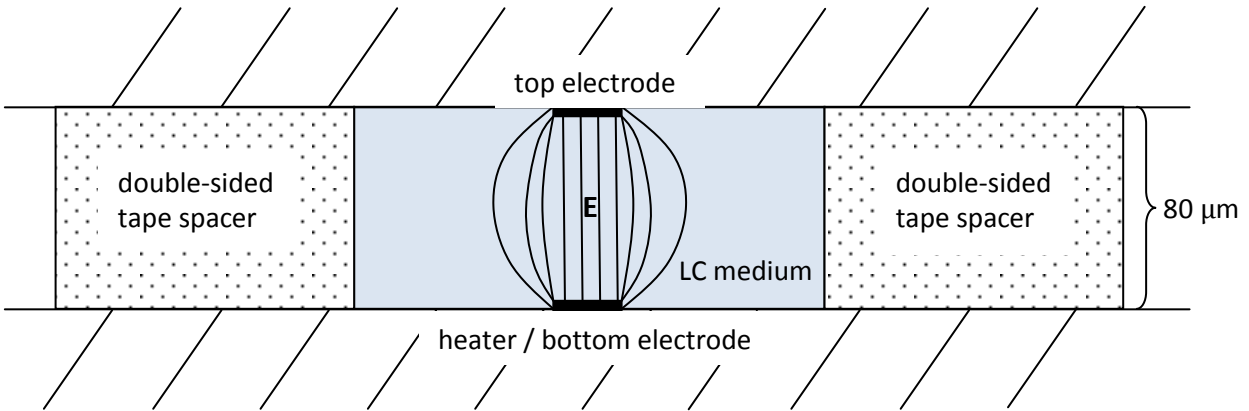


**Fig. 9** A side view of a filled cell. The double-sided tape spacers have a thickness of  $80\ \mu\text{m}$  which determines the thickness of the LC film. Because we apply voltage across two thin metal strips significant field edge effects will permeate the LC medium. The glass substrates, indicated by diagonal lines, have thicknesses of  $1\text{mm}$  and extend far beyond the cell dimensions.

The tape thickness, which determines the cell thickness, is measured to be roughly  $80\ \mu\text{m}$ . The literature reports LC cells of thicknesses typically ranging between  $5$  and  $30\ \mu\text{m}$ , so our cell is relatively thick. However, this thickness is actually warranted by the  $3\omega$  measurements because the thermal penetration depth,  $\lambda$ , must be longer than the heater half-width,  $b$ . The heater half widths range from  $5$  to  $20\ \mu\text{m}$ , and so a cell thickness of  $20\ \mu\text{m}$ , for example, would theoretically not allow any thin line regime. In practice we do detect characteristic thin line  $3\omega$  behavior even when  $\lambda$  is slightly less than  $b$ , so it would be possible to make thin line regime measurements on a  $20\ \mu\text{m}$  thick cell, but this would greatly reduce the already short measurement frequency range from  $2 - 50\ \text{Hz}$ .

Once an empty cell is prepared it is fixed to a copper stage with heat sink grease, as shown in Fig. 10. The cell is later filled with the LC of choice. A silicone rubber heater under the copper stage is used to control the sample temperature. Probes connected to the lock-in outputs and inputs are brought to contact the heater contact pads.

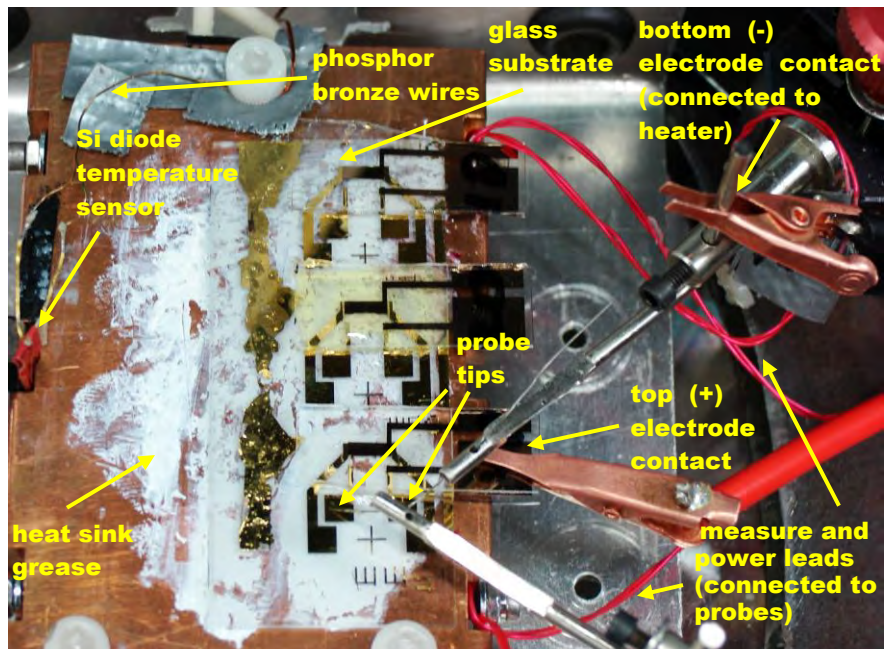


**FIG. 10** A close up of samples in measurement configuration. Three heaters (from top to bottom: 10  $\mu\text{m}$ , 20  $\mu\text{m}$ , and 40  $\mu\text{m}$ ) deposited onto a glass substrate are covered with top electrodes (of the same widths) and are fixed to a copper heating stage with heat sink grease. Measurement and power leads are connected to probes which make contact with the heater pads. A silicone rubber heater (not shown) lies beneath the copper stage to heat the environment. The presence of MBBA in the 20  $\mu\text{m}$  heater cell (center) gives it a yellowish hue.

## 6. Experimental Considerations

### 6.1 $3\omega$ Noise Floor

In principle, the  $3\omega$  signal should emerge with driving voltages as low as 1  $\mu\text{V}$ , but in practice we found that the characteristic  $3\omega$  behavior is measurable only for driving voltages on the order of 100 mV and above. This restriction to higher driving voltages is not due to an effect in the heater itself, but is instead a direct consequence of the  $3\omega$  content inherent in the voltage source. The left plot in Fig. 11 plots data of  $\Delta T$  vs.  $\ln(f)$  data measured with a 10  $\mu\text{m}$  wide Au-Ti heater on an empty cell. The linear relationship predicted by Eq. (10) is not obeyed at lower driving voltages because the  $3\omega$  signal produced by the heater interferes with the  $3\omega$  noise floor of the lock-in, which is found to be on the order of 10  $\mu\text{V}$ . We measure the  $3\omega$  content of the lock-in itself by introducing a short in place of the sample. The right plot in Fig. 11 plots data of

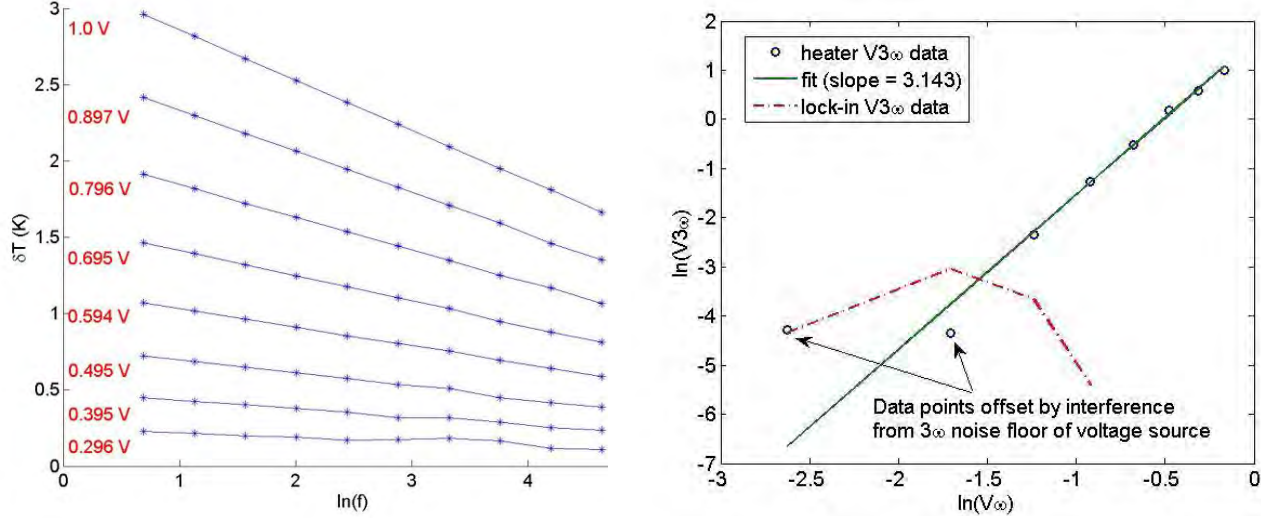


**FIG. 11** Two demonstrations of  $3\omega$  noise floor interference at low driving voltages. Left: Plots of temperature oscillation  $Re[\Delta T]$  vs.  $\ln(f)$  for various heater powers using a  $10 \mu\text{m}$  wide Au heater on an empty cell. The voltages across the heater are shown to the left (in red) of their respective plots. Lines connect the points for visual aid. The three lowest plots at the lowest powers deviate from the expected linear behavior because  $V_{3\omega}$  approaches the  $3\omega$  noise floor of the lock-in. Right: A plot of  $\ln(Re(V_{3\omega}))$  vs.  $\ln(V)$  should have a slope of 3. The fit, with a slope near 3, does not include the first 2 data points. At lower voltages the  $3\omega$  content inherent in the voltage source becomes larger than the signal produced by the heater and the data deviates from the predicted behavior due to interference between the two  $3\omega$  signals.

$V_{3\omega}$  vs.  $V$  for the lock-in over data of  $V_{3\omega}$  vs.  $V$  measured with a  $20 \mu\text{m}$  heater on an empty cell. If we combine the first term of Eq. (10) and the last term of Eq. (6) we find that

$$Re[\Delta T] = \frac{2Re[V_{3\omega}]}{\alpha V} = -\frac{V^2}{2\pi l \kappa} \ln(\omega) \quad (12)$$

A log-log plot of  $Re|V_{3\omega}|$  vs.  $V$  should then have a slope of 3 because  $Re[V_{3\omega}] \propto V^3$ . We expect a slope of +3 rather than -3 because  $Re[V_{3\omega}]$  is experimentally found to always be negative. Clearly, the first two points do not lie on the straight fit line that relates  $V$  to  $V_{3\omega}$ . The phase of the  $3\omega$  noise floor signal may interfere both constructively and destructively with that of the  $3\omega$  signal from the heater-thermometer, which is why one of the data points is above the fit line while the other is below it. In fact the phase of the  $3\omega$  noise floor is observed to jump over  $180^\circ$  between nearby frequencies causing the real part of the  $3\omega$  noise floor to become negative. The presence of the  $3\omega$  noise floor interference leads us to adjust the driving voltage of any given heater so that  $V_{3\omega}$  is on the order of 1 mV for high frequencies and safely distant from the  $3\omega$  noise floor.

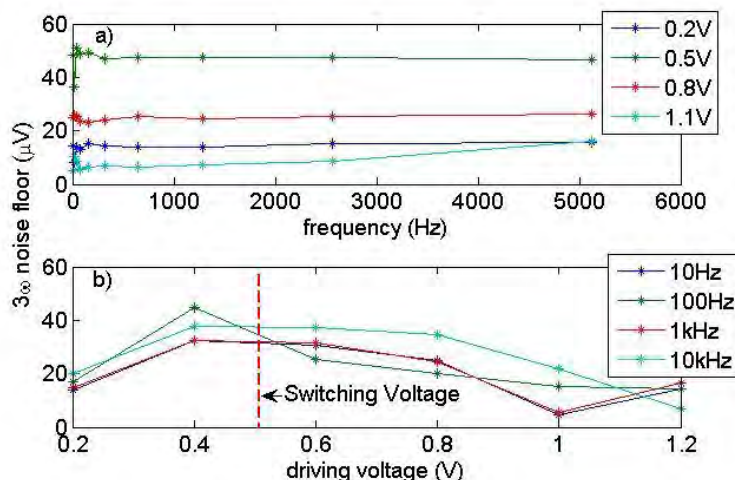


**FIG. 12** a) Frequency dependence of  $3\omega$  noise floor at various voltages. The  $3\omega$  content is very noisy at low frequencies, but becomes nearly constant above about 200 Hz. b) The  $3\omega$  content increases with voltages until the switching voltage (0.51 V) is reached, at which a relay in the voltage source switches to a set of resistors that produce lower  $3\omega$  noise.

Fig. 12 demonstrates the nontrivial dependence that the  $3\omega$  noise floor has on both voltage and frequency. Not clear from Fig. 12 a) is that the  $3\omega$  noise floor wildly oscillates as a function of frequency for frequencies  $< 200$  Hz. From Fig. 12 b) we see that the  $3\omega$  content of the lock-in increases with driving voltage until 0.51 V, after which it begins to decrease. This is because the voltage source of the lock-in amplifier has a built in relay switch that switches at 0.51 V to another set of resistors [15]. Evidently the resistors for the higher voltage range produce smaller  $3\omega$  noise than those for the lower range. Thus, in addition to producing a higher  $V3\omega$  signal from the heater, higher driving voltages also possess less  $3\omega$  noise, which gives us a second reason for choosing to use higher driving voltages. The presence of the  $3\omega$  noise floor was also noted in a recent paper by Syed Ahmed *et. al.* [22], but any mention of it is curiously absent from other papers that utilize a lock-in [13][14].

## 6.2 Determination of Frequency Range

We must determine the frequency ranges for which the thermal penetration depth,  $\lambda = \sqrt{D/(4\pi f)}$ , is in the thin line ( $\lambda \gg b$ ) regime for a given heater. Organic liquids typically have low thermal diffusivities [10] ( $D = \kappa/C_p$ ) on the order of  $D \approx 10^{-7}$  m<sup>2</sup>/s. Knowing this we can estimate the penetration depth as a function of frequency. In the thin line regime  $\lambda$  should be shorter than the 80 μm thickness of the sample but still longer than the heater half-width,  $b$ . For a 20 μm wide heater the thin line regime frequency range is chosen to be 2 Hz where  $\lambda \approx 40$  μm  $<$  cell thickness) to 50 Hz (where  $\lambda \approx 15$  μm  $>$   $b$ ). A plot of  $\lambda$  vs  $f$  (Fig. 13) allows for a quick determination of the appropriate frequency range.

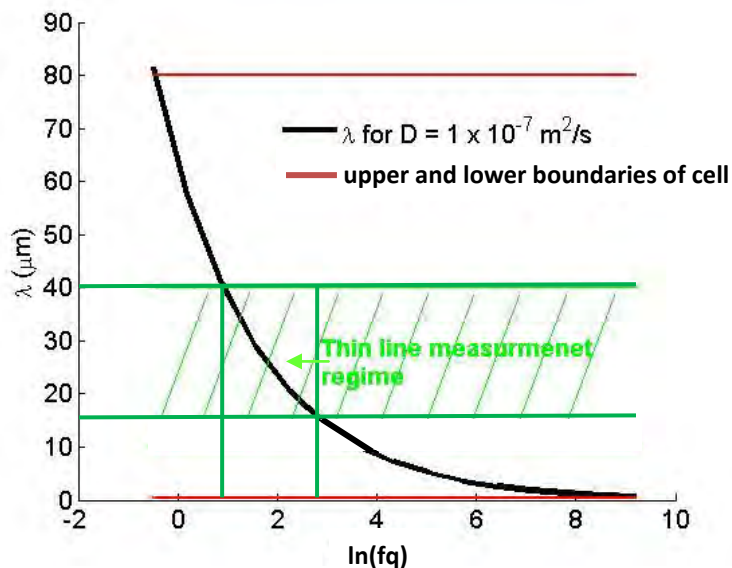


**FIG. 13**  $\lambda$  is plotted from 0.3 Hz to 4 kHz against  $\ln(fq)$ . The red lines are the upper and lower boundaries of the LC thin film. For  $\lambda > 80 \mu\text{m}$  (cell thickness) the heat wave encounters the top electrode and the boundary effect distorts the  $3\omega$  behavior. For  $\lambda < 320 \text{ nm}$  (heater thickness) the heat wave stays entirely within the heater itself, thus measuring  $\kappa$  of the heater, not the LC. The vertical green lines delineate the chosen thin line measurement regime (2 Hz to 50 Hz) for a  $20 \mu\text{m}$  wide heater that satisfies the theoretical constraints  $b < \lambda < \text{cell thickness}$ . The horizontal lines indicate the  $\lambda$  at the limits of the thin line measurement regime.

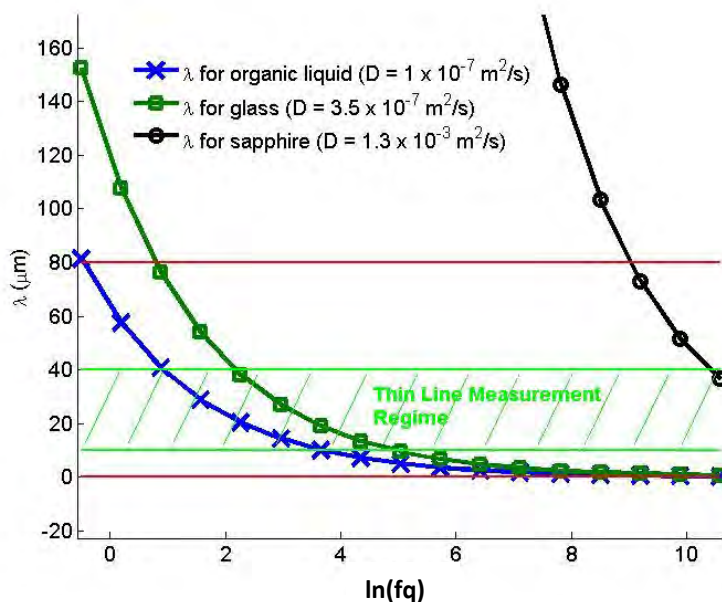
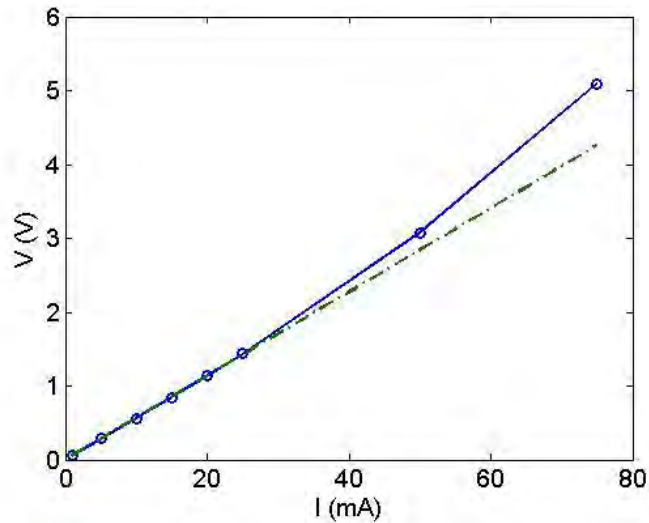


**FIG. 14** Plots of  $\lambda$  vs.  $\ln(fq)$  over a frequency range 0.3 Hz to 40 kHz for organic liquid, glass, and sapphire. The thermal penetration depth in glass for the 20 Hz to 50 Hz range is close to that of organic liquids, falling well within the 1 mm glass substrate thickness. The sapphire curve dwarfs the other two. The sapphire substrate would have to be over 8 mm thick if we were to measure its  $\kappa$  simultaneously with that of an organic liquid thin film.

Because the heater is deposited onto a substrate we must also consider the thermal penetration depth into the substrate. Fig. 14 presents  $\lambda$  vs.  $fq$  for organic liquid, glass, and sapphire. The thermal diffusivity of glass is close to that of an organic liquid and so the two curves are close together. The curve for sapphire dwarfs the other two within the 2 Hz to 50 Hz frequency range due to its much higher thermal diffusivity ( $D_{\text{sapph}} = 1.3 \times 10^{-3} \text{ m}^2/\text{s}$ ). An extension of the sapphire curve reveals that the sapphire substrate would have to be over 8 mm thick to be longer than the  $\lambda$  produced in the 20 Hz – 50 Hz measurement range. Given that sapphire is quite expensive, it would be an unreasonable choice for a substrate on which to measure LC thermal properties with the  $3\omega$  method. In general a substrate should be chosen such that the penetration depths for the frequency range chosen to measure the sample will fall well within a reasonable substrate thickness.

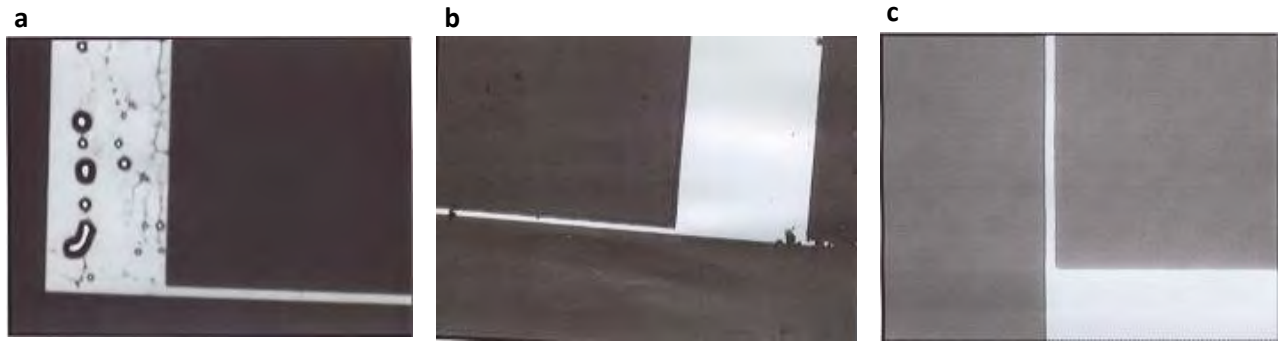
### 6.3 Staying in the Linear I-V Regime

The mathematical analysis of the  $3\omega$  method depends on the assumption that I and V are linearly related through Ohm's law, but this assumption breaks down when the current is too high. To determine the linear I-V regime the voltage was measured across a  $40 \mu\text{m}$  heater as current was increased. The I-V plot (Fig. 15) begins to deviate from linear regime above 30 mA. Most measurements were performed with about 20 mA of current running through the sample and were therefore within the Ohm's law regime. Such relatively high currents were needed so that the  $3\omega$  signal is well above the  $3\omega$  noise floor, described in section 6.1.



**FIG. 15** An I-V curve for a  $40 \mu\text{m}$  heater shows that the linear relationship of Ohm's law breaks down for currents above 30 mA.

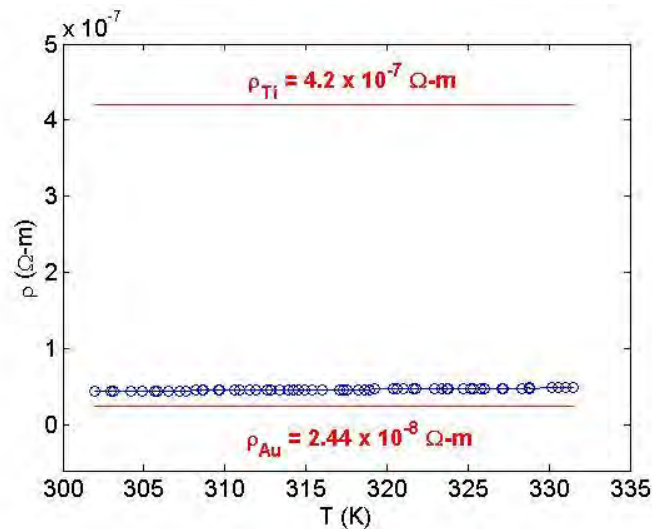
## 6.4 Heater Defects



**FIG. 16** All pictures show the region where the heater connects to the contact pad legs. a) Bubbles and cracks form on this 20  $\mu\text{m}$  heater (shown at 5x magnification) after liftoff is performed. b) Sometimes the high power acetone jet may remove poorly adhered chunks or even entire heaters. The black feature that appears to be a break in this 10  $\mu\text{m}$  heater (shown at 5x magnification) is actually a photoresist/metal flake that has stuck to the heater. c) A pristine 10  $\mu\text{m}$  heater (shown at 10x magnification) shows no obvious defects.

Photolithography processing never produces an exact replica of the mask, which itself is never an exact replica of the original computer generated design. It is therefore necessary to inspect the heaters for any obvious defects that will cause it to deviate from the theoretical behavior of a long, thin strip. Fig. 16 shows two kinds of defects commonly encountered in the fabrication process as well as an apparently defect-less heater.

Even if the heaters appear well resolved without any residues present on the surface (as in



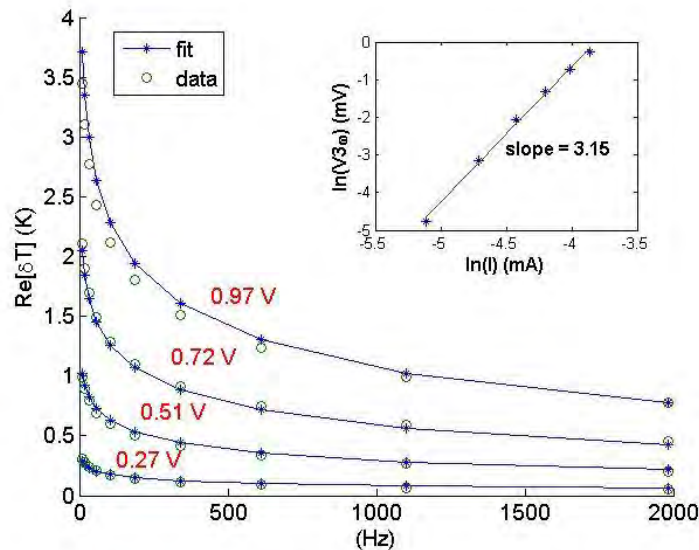
**FIG. 17** Red horizontal lines indicate the resistivity of Ti and Au. The blue connected circles are the measured resistivity vs. T of a 20  $\mu\text{m}$  heater. The heater resistivity is just over twice that of Au.

Fig. 16 c) the presence of internal defects may still substantially alter the flow of current. The heater lines are close to 310 nm thick, which is thick enough that size effects should not substantially alter the resistivity of the lines from their bulk values. Because the lines contain only a 10 nm thick layer of Ti, their resistivity should be close to that of gold. The resistivities of the lines are calculated from the measured resistance and knowledge of the approximate geometry. As is evident from Fig. 17, the resistivity of a 20  $\mu\text{m}$  line is roughly twice the bulk value of gold and nowhere near that of Ti. We do not expect the heater resistivity to be exactly equal to that of Au, but if it were an order of magnitude off we would not use the heater.

## 7. Experimental Procedure

### 7.1 Preliminary Tests

Before measurements of  $\kappa$  are performed we must assure ourselves that the heater signals follow Eq. (10). A quick measurement of  $V3\omega$  vs.  $fq$  is run in order to confirm that  $V3\omega$  is linear in  $\ln(fq)$ . Next  $V3\omega$  is measured against  $V$  to see if the cubic behavior predicted by Eq. (12) is obeyed. Fig. 18 shows data for a heater that has passed these preliminary tests. Of course, the voltage measured across the heater should also scale linearly with the voltage output by the lock-in amplifier. As the  $3\omega$  signal magnitudes from different heaters vary from 100  $\mu\text{V}$  to over 2 mV the optimal lock-in measurement range must always be determined before starting actual



**FIG. 18** Preliminary tests to confirm  $3\omega$  behavior. Data from a 20  $\mu\text{m}$  Au line heater on a glass substrate is compared to Eq. (10) for various heater powers. Eq. (9) is numerically integrated in MATLAB<sup>®</sup> with actual values of  $P$ ,  $l$ , and  $b$ .  $C_p$  and  $\kappa$  are adjusted until the fit is good for all plots ( $C_p = 2200 \text{ kJ/m}^3\cdot\text{K}$  and  $\kappa = 1.8 \text{ W/m-K}$  give good results). The inset shows a loglog plot of  $V3\omega$  as a function of driving current for the same line. A slope near 3 reassures us that  $3\omega$  behavior is occurring.

measurements. The frequency range for  $V_{3\omega}$  vs.  $f$  measurements is a logarithmic scale from 2 Hz to 4 kHz with 15 frequencies total. The first 10 frequencies fall within the 2 Hz to 50 Hz thin line measurement regime, while the last 5 extend into the planar regime. Data is only analyzed for the first 10 points, but the extended frequency range allows us to confirm the expected transition into the planar regime.

## 7.2 Measurements of $\kappa$ vs. T

If preliminary tests confirm the  $3\omega$  behavior we proceed to measure the temperature dependence of  $\kappa$  for the empty cell. The temperature range is chosen to cover the phase transitions of the LCs that will be measured after filling the cell. For 5CB ( $T_{NI} \approx 305$  K) this range is chosen to be 295 K to 316 K, while for 8CB ( $T_{SmN} \approx 303$  K,  $T_{NI} \approx 314$  K) and MBBA ( $T_{NI} \approx 318$  K) it is 300 K to 331K. The temperature controller is set to a step size of 0.5 K. The temperature ramp rate is set to a fairly slow 0.1 K/min so as to avoid any significant convection within the LC medium. At each temperature step the lock-in amplifier measures the voltage across the heater and  $\text{Re}[V_{3\omega}]$  vs.  $f$ . The multimeter measures the voltage across a  $5 \Omega$  precision resistor in series with the sample, determining the current in the sample. Because we do not have a cooling system installed, it takes some time for the temperature to stabilize at each step. Combined with the slow ramp rate, the  $\kappa$  vs. T measurements typically take over 6 hours to complete. Fig. 19 depicts the instrumentation used for this measurement.

Once measurements of the empty cell are completed the cell is filled with MBBA, 5CB, or 8CB by capillary action and the  $\kappa$  vs. T measurements are repeated. The presence of the LC always reduces the  $3\omega$  signal magnitude so there is no signal overload danger if measurement settings are left unchanged from those used for the empty cell. All measurements are controlled

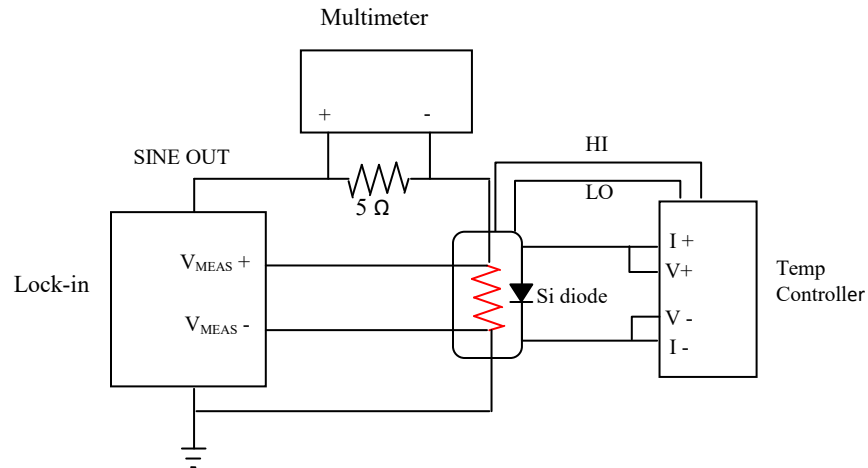


**FIG. 19** A schematic of the instrumentation used during measurement. The lock-in uses a 4 point configuration to measure  $V_{3\omega}$  across the heater (denoted as a resistor in red). The temperature controller uses a similar configuration to measure the resistance of the Si diode sensor and two separate leads control the silicone rubber heater. HI and LO leads from the temperature controller are connected to the silicone rubber heater. The multimeter measures voltage across a  $5 \Omega$  precision resistor.

with a LabVIEW™ 8.6 program installed on a Linux Kubuntu operating system. The data accumulated by LabVIEW is then loaded into MATLAB® 7.4 for analysis. LabVIEW and MATLAB codes are provided in the appendix.

### 7.3 Measurements of $\kappa$ vs. $V$

These measurements are made using the same instrumentation depicted in Fig. 19 with the addition of a DC voltage source (Keithley 617) connected to the top and bottom electrodes. The purpose of these measurements is primarily to detect alignment with an electric field in the nematic phase of MBBA, 5CB, and 8CB. The temperature is set near the middle of the nematic phase so that the oscillation of the temperature controller (typically about 0.3 K) will not bring the LC in and out of phase transitions. Measurements with and without DC voltage applied to an empty cell were verified to give the same results before any  $\kappa$  vs.  $V$  measurements were made on LC thin films, ensuring that application of a DC voltage does not couple with the AC field within the heater to produce spurious  $3\omega$  signals.

## 8. Results and Discussion

We present the measured temperature and voltage dependence of the thermal conductivity of MBBA, 5CB, and 8CB thin films. Expected  $\kappa$  behavior is detected in most of the measurements, but we find that the 5CB data gives the cleanest results. The origins of some of the measurement difficulties are discussed throughout this section along with clear suggestions for improvement in future experiments.

### 8.1 Temperature Dependence of Thermal Conductivity

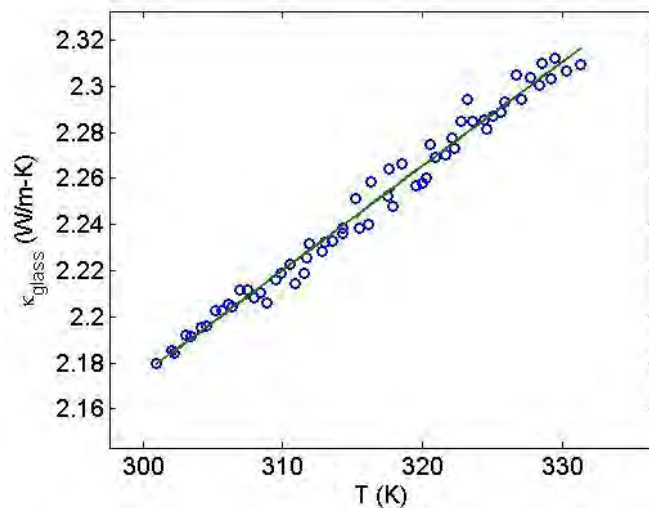


**FIG. 20** As expected, the thermal conductivity of the glass substrate increases linearly with temperature. However, the magnitude seems to be twice that of the literature value.

### 8.1.1 Glass

Before filling cells with the LCs the thermal conductivity of the empty cell must be measured. Fig. 20 shows that the measured  $\kappa$  increases linearly with temperature, which indeed is a characteristic of glass [25]. Because measurements are not made in vacuum, we must use the literature value of the thermal conductivity of air ( $\kappa_{\text{air}} = 0.025$  W/m-K) [25] to subtract it from the total measured  $k$  in order to isolate  $\kappa_{\text{glass}}$  according to Eq. (11). Unfortunately, the magnitude of  $\kappa_{\text{glass}}$  is twice the value reported in the literature (1.1 W/m-K at room temperature). This factor of 2 is addressed later on in this section.

### 8.1.1 MBBA

$\kappa_{\text{MBBA}}$  vs.  $T$  was measured 4 times. One of these data sets is used to produce Fig. 21. As described above,  $\kappa_{\text{glass}}$  is obtained by subtracting  $\kappa_{\text{air}}$  from the empty cell data.  $\kappa_{\text{MBBA}}$  is then isolated by subtracting  $\kappa_{\text{glass}}$  from the filled cell data. Fig. 22 zooms in on the  $\kappa_{\text{MBBA}}$  data alone. The literature [3] usually reports a nematic isotropic transition temperature of  $T_{\text{NI}} = 318$  K. But  $T_{\text{NI}}$  is actually thickness dependent [4][23] and thus liable to shift by a few Kelvin from this value, so Fig. 22 indicates an approximate range in which we expect to detect the N-I phase transition. Unfortunately, a discontinuity characteristic of a phase transition was not observed in any of the MBBA measurements. This is most likely due to poor alignment in the nematic phase of MBBA. Crisscrossing surface grooves and the presence of contaminants may disrupt the long-range order in the nematic phase. Glass substrates intended for MBBA use were etched so as to induce homeotropic alignment (the reasoning is described in section 4.2). It is likely that the etching did not produce the desired alignment effect and instead induced substantial disorder, as the nematic phase is highly sensitive to surface treatments [20]. Marinelli *et al* [24] explain that

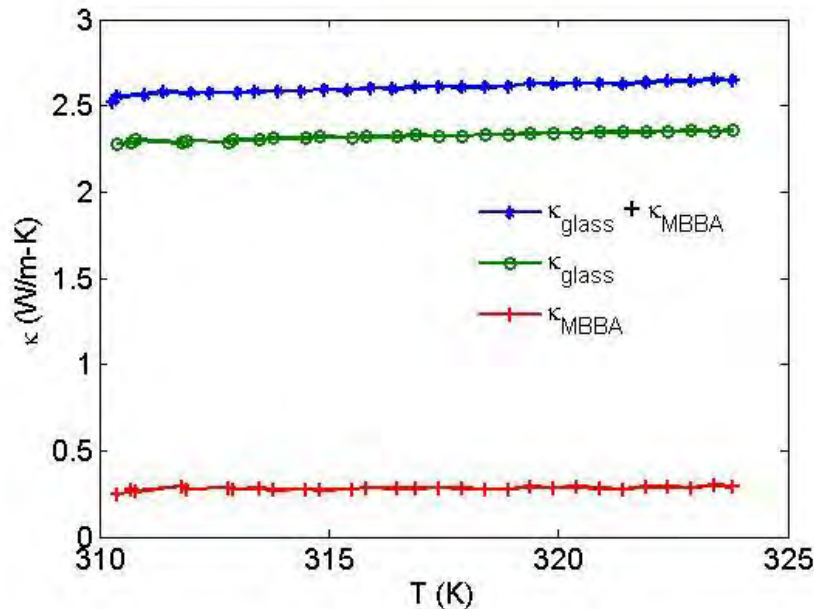
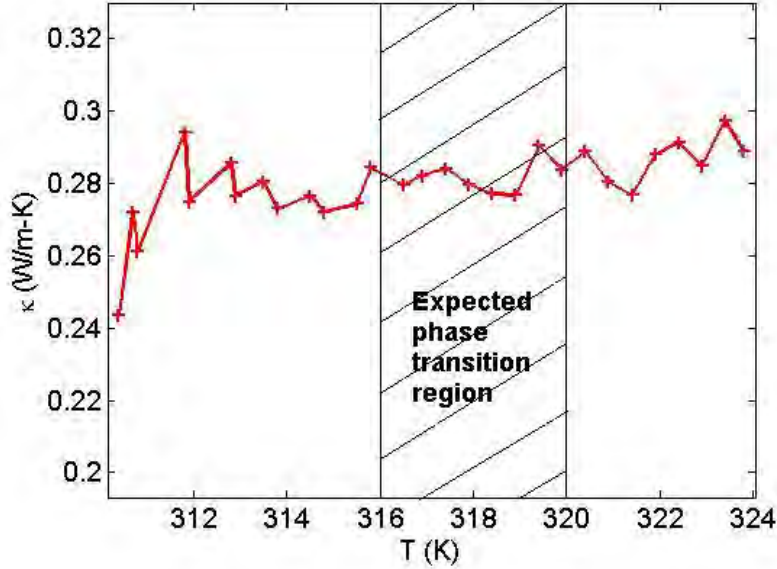


FIG. 21 Glass data is subtracted from the filled cell data to isolate  $\kappa_{\text{MBBA}}$  vs  $T$ .



**FIG. 22** The  $\kappa_{\text{MBBA}}$  vs.  $T$  data does not exhibit any clear phase transition behavior. This is likely due to poor alignment in the nematic phase and long  $V3\omega$  vs.  $f_q$  measurement times that do not resolve short lived phase behavior.

the thermal conductivity for unaligned molecules in the nematic phase can be fit by a linear function in  $T$ ,  $(\kappa_{\parallel}(T) + 2\kappa_{\perp}(T))/3$ , where  $\kappa_{\parallel}$  and  $\kappa_{\perp}$  are the thermal conductivities parallel and perpendicular to the major molecular axis. When this fit line is evaluated for higher temperatures it actually matches  $\kappa$  in the isotropic phase. Thus  $\kappa$  lies on the same line in both nematic and isotropic phases when surface alignment is poor.

Even if surface alignment is poor a small spike is still expected at the phase transition. It is quite possible that the time resolution of the measurement was too coarse to resolve a small spike at the transition. The thermal conductivity is not measured in an instant, but is the result of measurements of  $V3\omega$  vs.  $f_q$ , which take about 1.5 min each. Reducing the  $V3\omega$  vs.  $f_q$  measurement time so as to detect short-lived phase transition behavior requires adjustment of the measurement parameters. For example, thinner heaters can be used so that the thin line measurement regime is pushed to higher frequencies. At higher measurement frequencies the time constant can be reduced from the rather lengthy 1 s used for the present measurements, allowing a quicker phase-locking of the lock-in amplifier, and hence reducing the  $V3\omega$  vs.  $f_q$  measurement time. Furthermore, it should be noted that the work presented here is in a sense only half complete, as operation of heaters in the planar regime was not attempted. In the planar regime, measurements give the specific heat, which is highly responsive to phase transitions, at high frequencies and thus would easily be able to detect a short-lived phase transition. An ideal high frequency measurement would measure  $V3\omega$  vs.  $f_q$  as temperature slowly ramps rather than waiting for temperature to stabilize at a set point to take a measurement.

### 8.1.3 5CB

Measurements of  $\kappa$  vs.  $T$  are performed on two cells with two different  $20\ \mu\text{m}$  heaters. Unlike the MBBA measurements, both of these measurements, shown in Fig. 23, exhibit

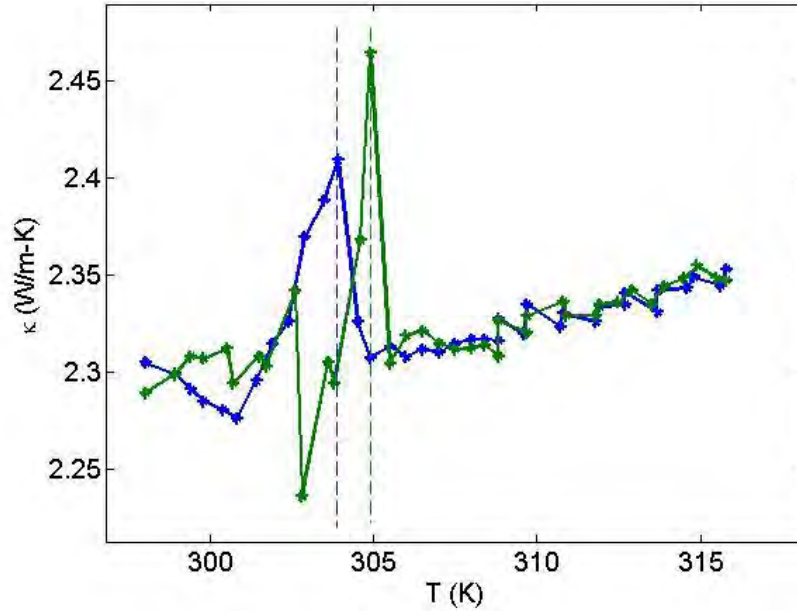


**FIG. 23** Data taken for two different 5CB cells. Lines help follow the behavior of  $\kappa$ . It is clear that  $T_{\text{NI}}$  (indicated by dotted lines) is not exactly the same for both measurements. Noisiness near the phase transition is likely due to the fact that the temperature oscillates about the transition temperature and the LC molecules switch back and forth between nematic and isotropic phases.

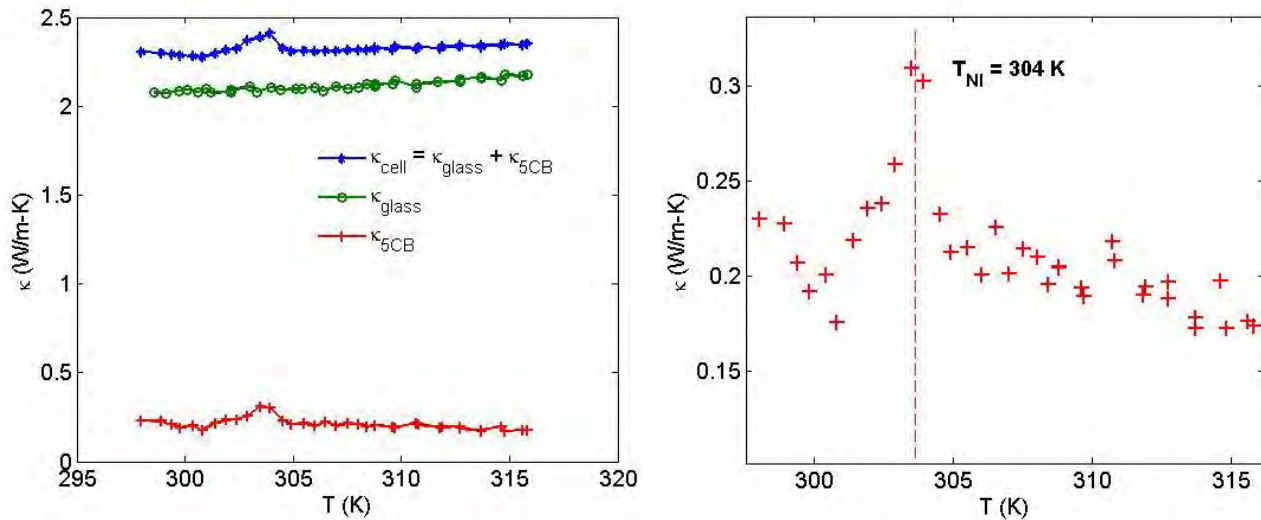


**FIG. 24** The data exhibits a negative slope in the isotropic phase, which agrees with earlier measurements [7][24]. We expected the magnitude of the measured  $\kappa_{5\text{CB}}$  in the isotropic phase ( $0.238\ \text{W/m-K}$ ) to be twice as large as the reported value ( $\sim 0.15\ \text{W/m-K}$ ) due to the multiplicative factor of 2 in the  $\kappa_{\text{glass}}$  measurements, but it is only 1.58 times larger.

noticeable N-I phase transition behavior. It is clear that the nematic-isotropic transition temperature,  $T_{NI}$ , is not exactly the same for both measurements. This is expected, as the mesophase transitions are gradual, taking place over approximately 40 s. In fact the phase transition can be seen with the naked eye. As the temperature nears the critical region the isotropic phase approaches from the edges and slowly engulfs the entire sample, changing its appearance from milky white to clear.

We take one of the data sets (blue in Fig. 23) and subtract the  $\kappa_{\text{glass}}$  data from the total  $\kappa_{\text{cell}}$  data in order to isolate  $\kappa_{5CB}$ . The right plot in Fig. 24 shows  $\kappa_{\text{glass}}$ ,  $\kappa_{\text{cell}}$ ,  $\kappa_{5CB}$  vs  $T$  and the left plot zooms in on the  $\kappa_{5CB}$  data. The measured  $\kappa_{5CB}$  decreases with temperature in the isotropic phase, a behavior similar to that presented in previous papers [7][24]. These papers reported  $\kappa_{5CB} = 0.15$  W/m-K just after the N-I phase transition. As our  $\kappa_{\text{glass}}$  measurements are scaled by a factor of 2, we expected our  $\kappa_{5CB}$  results to do the same. In this particular measurement the first point in the isotropic phase is measured to be 0.238 W/m-K, which is roughly 1.6, not 2, times larger than the literature value. As our aim is ultimately to determine the operational (nematic) range of a thin film heat-switch, we are satisfied with result. Between 4 separate measurements, the N-I transition temperature was found to be  $T_{NI} = 304.13$  K.

#### 8.1.4 8CB

We detect both the Sm-N and the N-I phase transitions in only one 8CB sample, the data for which is presented in Fig. 25. All other samples exhibited phase transition behavior at  $T_{SmN}$  but not at  $T_{NI}$ . It is possible that the same alignment problems described in section 8.1.2 are responsible for the absence of  $T_{NI}$  behavior for these measurements as well. The procedures for

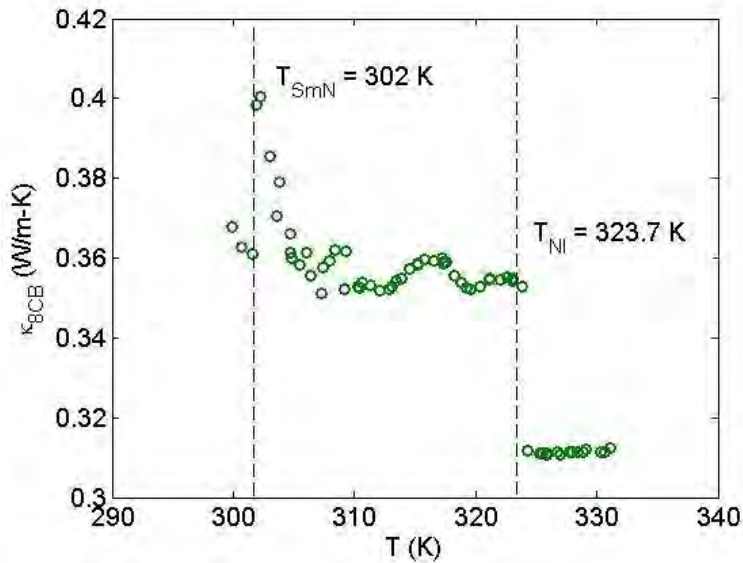


**FIG. 25**  $\kappa_{8CB}$  is measured through the smectic A-nematic and nematic-isotropic phase transitions. The sharp drop in  $k$  at  $T_{NI}$  indicates that the 8CB molecules were in fact homeotropically aligned near the surface.

isolating  $\kappa$  have already been described above, so Fig. 25 shows  $\kappa_{8CB}$  vs  $T$  alone. Marinelli [24] reports values of  $\kappa_{8CB}$  near 0.16 W/m-K just after the NI phase transition. Our values are close to 0.31 W/m-K (1.94 times larger), which is surprisingly almost exactly the factor of 2 that we expect.

The sharp drop in  $\kappa$  at  $T_{NI}$  indicates that the 8CB molecules were in fact homeotropically aligned (standing up) near the surface. Had they been homogeneously aligned (lying down)  $\kappa$  would in fact be lower in the nematic state than the isotropic state [24]. This is easily understood, as  $\kappa$  of the isotropic state,  $(\kappa_{\parallel} + 2\kappa_{\perp})/3$ , is a combination of both alignments and  $\kappa$  is greater along the molecular major axis than perpendicular to it. In order to better support such conclusions, future measurements should be performed as the LC alignment is optically monitored.

## 8.2 Measurements of Thermal Conductivity Anisotropy

### 8.2.1 Glass

Before measuring  $\kappa$  vs.  $V$  for the LC samples we must assure ourselves that application of the DC field does not couple with the  $3\omega$  signal as it is to be used solely as an alignment mechanism. This is done by applying voltages across an empty cell. A plot of  $R$  vs.  $V$  (see Fig. 26) for a 20  $\mu\text{m}$  heater reveals that a sudden 1.25 % drop in the data occurs when the DC voltage source is turned on. We calculate that a change in  $R$  of 1.25 % results in a change in  $\kappa$  of 1.32 % and therefore a small error is introduced to our measurements.

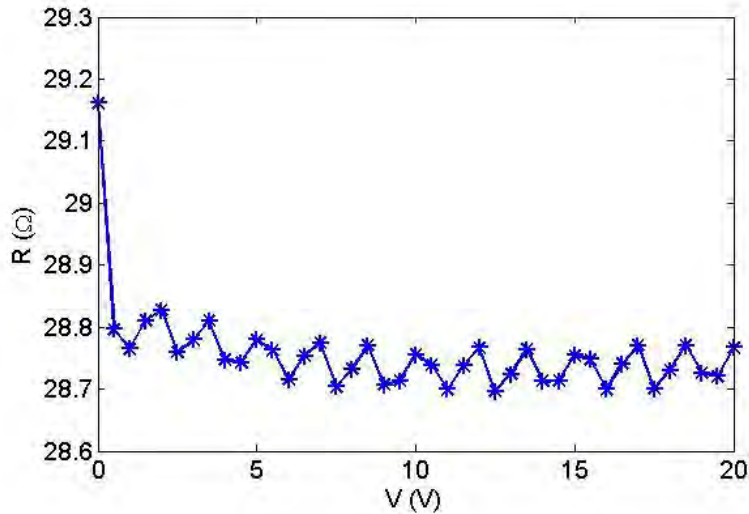


**FIG. 26** A plot of the  $R$  vs  $V$  data measured for an empty cell. A drop in  $R$  of 1.25 % occurs when the DC voltage source is turned on.  $R$  stays relatively constant as the voltage across the cell is increased. The sawtooth appearance is due to the temperature oscillations of the temperature controller.

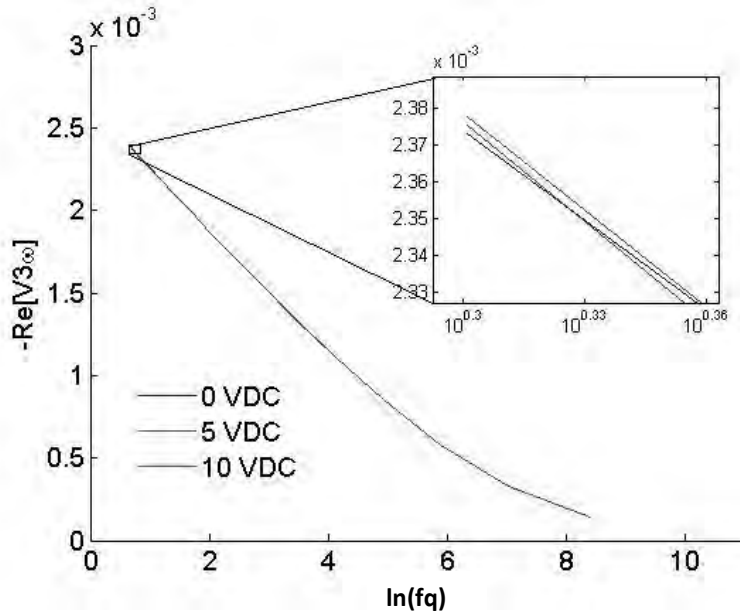


**FIG. 27** Plots of  $V3\omega$  vs.  $fq$  for 0V, 5 V, and 10 V applied across an empty cell. The application of a field does not have significant effect on the  $3\omega$  profile as differences between the plots are on the order of tens of  $\mu\text{V}$  while the  $3\omega$  signal is on the order of mV.

Fig. 27 displays  $V3\omega$  vs.  $fq$  measurements taken with three different voltages (0 V, 5 V, 10 V) applied across the same empty cell. The 5 V and 10 V plots cannot be resolved from the 0 V plot until we zoom a few orders of magnitude into the plots. The undisturbed  $3\omega$  profiles assure us that the DC field is safely decoupled from the AC field within the heater-thermometer, and does not give rise to spurious  $3\omega$  signals.

### 8.2.2 MBBA

DC voltage is applied across the heater (–) and top electrode (+) in order to align the LC molecules. Measurements of three different cells filled with MBBA were made at 310 K (well within the nematic phase) for different voltage ranges. Voltage is increased in relatively small steps (0.5 V) and  $V3\omega$  vs.  $fq$  measurements are spaced by 30 s in order to minimize any convection effects due to sudden field increases. The thermal conductivity of glass at 310 K was measured 5 times, giving a mean value of  $\kappa_{\text{glass}} = 2.24 \pm 0.1 \text{ W/m-K}$ . This value was then subtracted from the filled cell data to obtain the plots in Fig. 28. It is clear that they do not agree in magnitude. The LC molecules were probably badly aligned over the heater-thermometers, but were not entirely isotropic so that each cell exhibited a unique combination of  $\kappa_{\parallel}$  and  $\kappa_{\perp}$ . Combined with the measurement error which, for filled cell measurements, is found to be roughly 0.05 W/m-K, the magnitude differences are reasonable. What interests us more than precise magnitude measurements is the overall alignment behavior of MBBA. Each of the measurements exhibit a negative trend with applied voltage, which is expected because MBBA

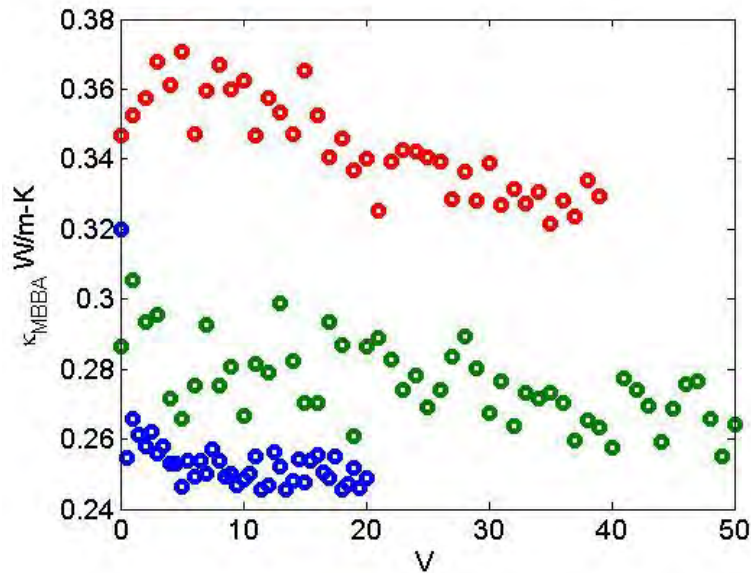


**FIG. 28** Measurements of  $\kappa_{\text{MBBA}}$  vs  $T$  from three different cells were taken with different voltage ranges. They all clearly exhibit a negative trend which is expected as MBBA possesses a negative  $\Delta\epsilon$ . Obviously the data differ substantially from each other in magnitude. This is probably due to variations in molecular alignments between the 3 cells. Bad surface alignment is probably also responsible for the very small field alignment effect. No Freedericksz transition behavior is detected.

(with negative  $\Delta\epsilon$ ) tends to align perpendicular to an applied field and  $\kappa_{\perp} < \kappa_{\parallel}$ . The alignment effect, though consistent, is unfortunately quite small. We attribute this once more to the lack of uniform homeotropic surface alignment, which is necessary to measure the full anisotropy of  $\kappa_{\text{MBBA}}$ .

### 8.2.3 5CB

Strong voltage alignment effects were detected in several 5CB cells. Fig. 29 shows three measurements of a single 5CB cell at 294 K made by a 20  $\mu\text{m}$  wide heater. The Freedericksz transition, which is described in section 1.4, is clearly observed in all three measurements, with alignment beginning at a critical field of approximately 5 V. The increasing  $\kappa_{5\text{CB}}$  indicates gradual alignment of molecules with the field. As the field increases past the maximum strength used in these measurements the curve will saturate at the value of  $\kappa_{\parallel}$ , which we estimate to be 0.308 W/m-K.  $\kappa_{\perp}$  is calculated by taking the average of the three measurements at  $V = 0$ , giving  $\kappa_{\perp} = 0.209$  W/m-K. This gives a thermal conductivity anisotropy of  $\Delta\kappa = 0.099$  W/m-K and a thermal conductivity contrast ratio of  $K = 1.47$ . The data informs us that if this cell were to be used as a thermal switching device, voltages of 20 V or greater would be required.

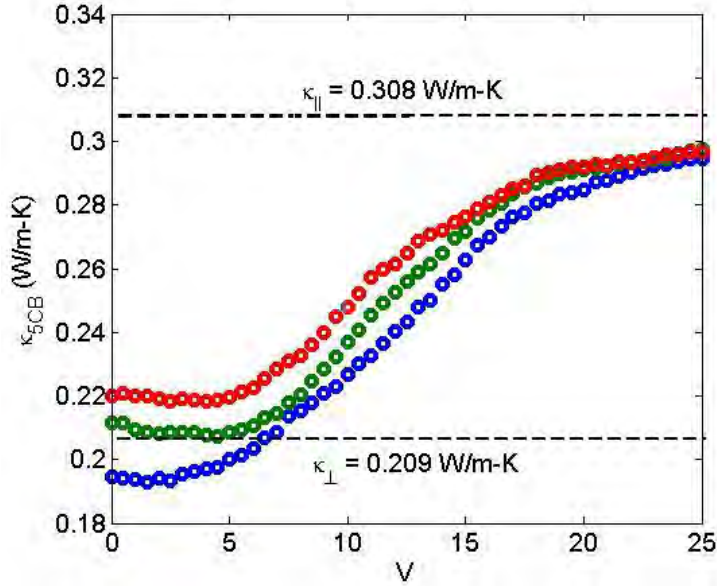


**FIG. 29** Three consecutive measurements on the same 5CB cell exhibit clear alignment behavior. The Fredericksz transition occurs approximately at  $V_C = 5$  V. At low field strength ( $V < V_C$ ) the molecules lay along the glass surface and the heat pulses generated by the  $20 \mu\text{m}$  heater line penetrate perpendicular to the molecular axis, thus measuring  $\kappa_{\perp}$ . We take the average of the three measurements at  $V = 0$  to present as  $\kappa_{\perp}$ . As the field strength increases the molecules begin to stand up. If we had extended the measurements to higher voltages we would have fully aligned the molecules and  $\kappa$  would cease to increase with  $V$ . Knowing the usual shape of alignment curves for LCs, we estimate a saturation line corresponding to  $\kappa_{\parallel}$ . This gives a thermal conductivity anisotropy of  $\Delta\kappa = 0.099$  W/m-K and a thermal conductivity contrast ratio of  $K = 1.47$ .

#### 8.2.4 8CB

Alignment effects were not detected in most of the 8CB cells. Fig. 30 shows two measurements of an 8CB cell in the nematic phase ( $T = 310$  K) that did show some reproducible behavior, but it does not echo the obvious Fredericks transition found in the 5CB data. Instead molecules appear to begin aligning at arbitrarily small field strengths. After about 5 V, however,  $\kappa_{8CB}$  begins to drop. It is possible that electrons from the surface of the ( $-$ ) electrode are flowing through the LC medium, as there is no insulating layer preventing them from doing so. The DC voltage source has a 2 mA current limit and will not register any errors for currents below this limit. Unfortunately, we did not monitor current flow through the LC medium during the course of these measurements to confirm or reject this suspicion. Earlier samples were actually produced with an evaporated layer of polyvinyl alcohol (PVA) coating the glass surfaces. The PVA layer was unidirectionally rubbed and intended for aligning the LCs. However, our evaporation process produced PVA layers pocketed with bubbles and crossed with ridges that would have introduced more disorder than order to the LCs near the surface and so PVA coating was discontinued. Rather than allowing PVA to evaporate onto the glass surfaces sitting on a hot

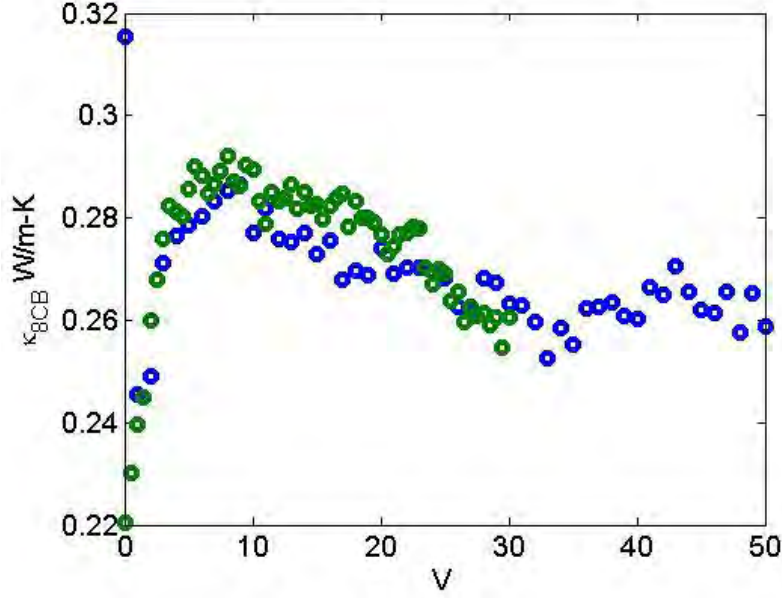


**FIG. 30** Two consecutive measurements of  $\kappa_{8CB}$  vs.  $V$  on a single 8CB cell.  $\kappa_{8CB}$  seems to increase rapidly with voltage until  $V \approx 5$  V, after which it begins to fall. The heater surfaces were not coated with any insulating alignment layer and were left in direct contact with the LC medium. The falling  $\kappa_{8CB}$  may be due to the appearance of a small discharge current across the thin film that prevents high enough electron build up at the (-) electrode for sufficiently strong aligning fields to be achieved.

plate, future samples should be prepared by spin coating the glass substrates with PVA so that the layers are flat with highly uniform thickness.

Measurements of  $\kappa_{8CB}$  vs.  $V$  were also made in the smectic A phase. These did not exhibit any reproducible alignment effects. In fact no alignment should be detected in this phase as it consists of layers of molecules with major axes already aligned perpendicular to the surface.

### 8.3 A Persistent Factor of 2

Papers on the  $3\omega$  technique [10][13][14] unanimously quote the solution of heat diffusion from an infinitely thin line into a surrounding medium as is presented in Eq. (7). and attribute the original solution to Carslaw and Jaeger [11]. However, inspection of the original text reveals that the expression for  $\Delta T$  is actually a factor of 2 smaller. The factor of 2 is almost certainly a consequence of the fact that Carslaw & Jaeger assumed the line to be imbedded in a uniform medium, while the solutions in the papers assume that heat diffuses only into the region below the heating line. With heat forced to diffuse through only one side of the heater it is no surprise that the temperature oscillations at the heater are twice as large, for half of the heat that could be diffusing away is not. This should not be a problem as the two sided approximation (Eq. (11)) is a combination of two one sided solutions. Furthermore, the diffusivity of LCs and glass are on the same order, and thus the thermal boundary resistance encountered during filled cell

measurements should be negligible. Nonetheless, the overshoot in  $\kappa$  persists and we consider numerous sources of experimental error that could account for this.

Earlier measurements were actually found to be a factor of 3 to 4 higher than the literature values. This discrepancy was found to be due to faulty resistance measurements which depended on knowledge of the exact output impedance of the lock – in amplifier. A simplified resistance measurement (described in section 3.3) gave more accurate results and reduced the overshoot to the current factor of 2.

### 8.3.1 Comparison with Numerical Solution

All the data presented in this thesis was calculated with the thin line approximation and not the exact solution. To check how much our measured  $3\omega$  signals deviated from the exact solution we plotted the raw data for an empty cell with a numerical evaluation of Eq. (8) on the same axes, using the measured value of  $\kappa$  in the numerical evaluation (left side of Fig. 31). The numerical solution predicts  $\Delta T$  of higher magnitude than what was measured, but  $\kappa$  is calculated from the slope of  $\Delta T$  vs.  $\ln(fq)$  which are in fact very similar. Therefore agreement is quite good. Changing  $\kappa$  to match the literature value of glass results in a substantial deviation between the

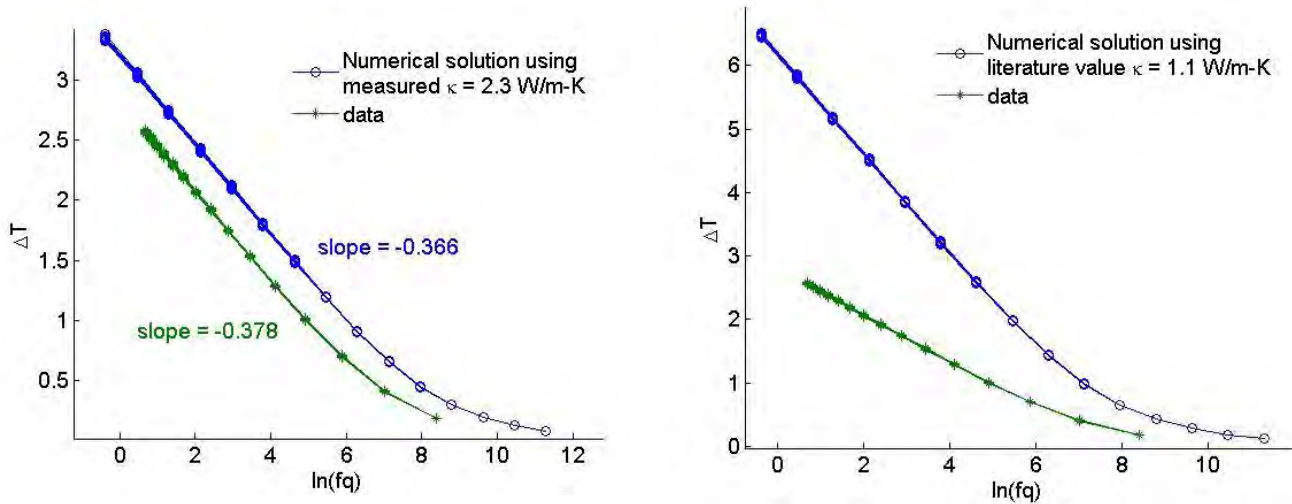


**FIG. 31** Left: The theoretical solution (blue) was evaluated for the  $V1\omega$ ,  $R$ , and  $\kappa$  obtained from analysis of the data (green) and a volumetric heat capacity  $C_p = 2200$  kJ/m<sup>3</sup>K typical of glass. Curves are plotted for each of the 43 temperature steps, giving a thickness to the plot due to the temperature dependence of  $\kappa$ . A heater width of  $40$   $\mu\text{m}$  and length of  $3.5$  mm was used (these are the dimensions that would result from a flawless heater fabrication). Although the theory predicts higher  $\Delta T$ , only the slope of  $\Delta T$  vs  $\ln(\omega)$  contributes to calculation of  $\kappa$ . A fit that would match the slope of the exact solution would therefore yield values of  $\kappa$  that are very near to those already plotted for glass in Fig. 20. Slopes are only calculated using the first 10 data points (thin line regime). Right: Changing  $\kappa$  to match the literature value for glass ( $1.1$  W/m-K) results in a significant change in slope. Another experimental parameter, such as  $V$ ,  $R$ , or  $\alpha$  would have to be varied in order to restore agreement between data and numerical solution.

data and the numerical solution. Parameters such as the heater length,  $l$ , and the temperature coefficient,  $\alpha$ , could be modified to restore agreement between the two curves, but these modifications were unphysical (cutting  $l$  in two or reducing  $\alpha$  by an order of magnitude, for example). We have not been able to pinpoint an experimental cause for the overshoot.

### 8.3.2 Factor of 2 as a Calibration Factor

It is interesting to ask if this factor scales in some way with the thermal conductivity, or if it remains 2 for all materials. We chose to deposit heaters onto a sapphire substrate which has a significantly higher  $\kappa$  than glass. Sapphire is an anisotropic material with  $\kappa_{\text{sapph}} = 35.1$  W/m-K parallel to optical axis and  $\kappa_{\text{sapph}} = 33.0$  W/m-K perpendicular to the optical axis at room temperature [26]. The heat waves generated by the heater flow radially outwards, and thus the measurements will give a combination of  $\kappa$  parallel and perpendicular to the optical axis. Because the sapphire substrates were polished on only one side photolithography proved to be quite difficult as UV backscattering would flood the patterns. However, after a series of modifications to the procedure (mostly reducing exposure and development times) heaters were successfully deposited. As mentioned earlier in section 6.2, the measurement frequencies had to be much higher than those used for the glass substrate due to the high thermal diffusivity of sapphire. The measurements of  $\kappa_{\text{sapph}}$  vs.  $T$ , shown in Fig. 32, were also apparently a factor of 2 higher than the literature values. The slope of  $\kappa_{\text{sapph}}$  vs.  $T$  is negative, which is in fact a property of sapphire. From the literature we calculate the slope to be  $-0.115$ . Dividing our data by 2 gives a slope of  $-0.105$ , which is only 9 % smaller. The persistent factor of 2 is in fact a welcomed result, as it suggests that our current measurement procedure can be calibrated by simply dividing by 2 in order to give accurate measurements of  $\kappa$ . Of course, our analysis is missing a thorough investigation of the solution of the heat equation from a thin line at the interface

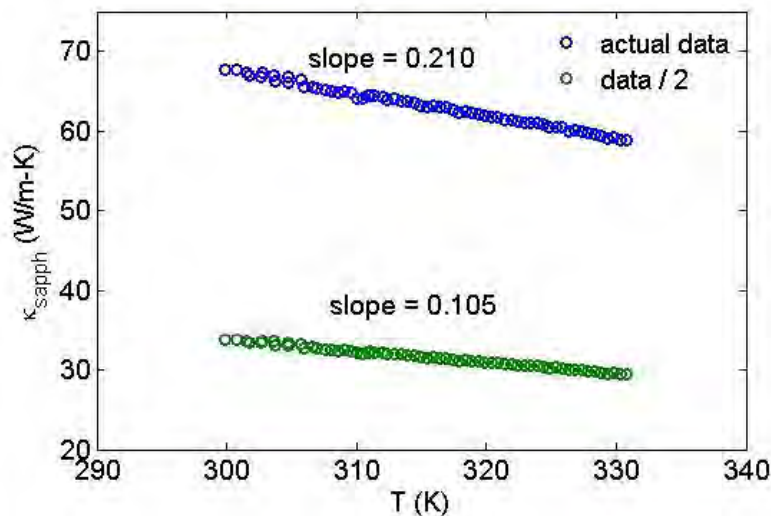


**Fig. 32** Measurements of  $\kappa_{\text{sapph}}$  vs.  $T$  seem to be a factor of 2 larger than literature values. When divided by 2 the slope of the data is 0.105, which is only 9 % smaller than that calculated from the literature.

between two different media. Although analytic solutions to this problem cannot be obtained [13], proper numerical methods can certainly give very close approximations. This was not attempted because the nature of the project was largely experimental and because time restrictions gave priority to other problems. For the present we are satisfied presenting the work as a calibrated thermal conductivity measurement.

## 9. Conclusion

The thermal conductivities of MBBA, 5CB, and 8CB have been measured as functions of temperature and alignment voltage with the  $3\omega$  method. In a sense this entire work has been a proof of concept, as the thermal characteristics of these materials are already known [24]. We have successfully demonstrated for the first time that a LC-based thermal heat switch can measure its own properties while in operation. Along the way we have described numerous improvements that can increase the effectiveness of the measurement technique. Future samples should be prepared in a cleanroom to avoid contamination. PVA should be spun onto the glass substrates so as to achieve consistent alignment and to insulate the LC medium from current leakage through the electrodes. Pushing measurements towards higher frequencies to better resolve short lived behaviors can be achieved by using thinner heaters and by measuring in the planar regime. In light of these improvements it is important for us to mention that the most significant aspect of this work may not be what has been done, but what can now be done with the knowledge we have accumulated. The efficiency of thin film heat engines increases with the thermal conductivity anisotropy of the heat switches [1]. Actual LC thin film switches may require newly synthesized LCs and/or LC mixtures that are optimized for wider temperature range operation and greater thermal conductivity anisotropy and whose thermal properties are as of yet unknown. Our calibrated measurement technique is well suited to thermally characterize these new materials.

## Acknowledgments

I would like to thank Kevin Malloy and Richard Epstein for introducing me to this project and guiding me along the way, Felix Jaeckel and Alex Albrecht for teaching me how to operate the lab instruments, Steve Wawrzyniec and Douglass Wozniak for their help with heater fabrication and constructing the measurement apparatus, and David Murrell for diagnosing Linux problems. Other than some machine work, all tasks pertaining to this project were performed by myself, though I received valuable assistance from fellow members of CHTM throughout the duration of the project. Construction of the measurement apparatus, mask design, and measurements of the  $3\omega$  noise floor were completed prior to officially beginning the honors thesis, but I included them here because they are vital aspects of the project as a whole.

## References

- [1] Epstein R. I., Malloy K. J., *J. Applied Phys. Phys.*, 106, 064509 (2009)
- [2] P. G. de Gennes, *The Physics of Liquid Crystals* (Clarendon Press, Oxford 1974)
- [3] S. Chandrasekhar, *Liquid Crystals* (Cambridge University Press 1977)
- [4] S Arumugam, S. V. Bhat, N. Kumar, K. V. Ramanathan, R Srinivasan, *Proc. Ind. Acad. Sci.*, Vol. 95 Nos 1 & 2 (1985)
- [5] A. Zidansek, G. Lahajnar, S. Kralj., *Appl. Magn. Reson.*, 27, 311 – 319 (2004) 8CB phase transitions
- [6] V. S. V. Rajan, J. J. C. Picot, *Mat. res. Bull.*, Vol. 9, pp. 311 – 318 (1974)
- [7] G. Ahlers, D. S. Cannell, L. I. Berge, and S. Sakurai, *Phys. Rev. E*. 49 (1), 545 (1993)
- [8] H. Kawamoto, *The History of Liquid Crystal Displays*, *Proc. IEEE*, Vol. 90, NO. 4, April 2002
- [9] J. Castellano, *Modifying Light*, *American Scientist*, September-October 2006
- [10] D. G. Cahill, *Rev. Sci. Instrum.* 61 (2), 808 (1990)
- [11] H. S. Carslaw and J. C. Jaeger, *Conduction of Heat in Solids* (Oxford University Press, 1959)
- [12] N. O. Birge and S. R. Nagel, *Rev. Sci. Instrum.* 58 (8), 1464 (1987)
- [13] I. K. Moon and Y. H. Jeong, *Rev. Sci. Instrum.* **67 (1)**, 29 (1996)
- [14] S. R. Choi, J. Kim, and Dongsik Kim, *Rev. Sci. Instrum.* **78 (8)**, 84902 (2007)
- [15] SR830 Operating Manual and Programming Reference (Stanford Research Systems 1993)
- [16] Lakeshore Model 330 User's Manual (Lake Shore Cryotronics 1994)
- [17] Keithley Model 2010 User's Manual (Keithley Instruments 1996)
- [18] Keithley Model 617 Programmable Electrometer Instruction Manual (Keithley Instruments 1984)
- [19] private communication with Steve Wawrzyniec
- [20] J. Cognard, *Molecular Crystals and Liquid Crystals*, Supplement 1 (Gordon & Breach, New York 1982)
- [21] Barmantlo, M. van Aerle, N. A. J. M. Hollering, R. W. J. Damen, J. P. M., *Journ. Appl. Phys.* 71 (10), 4799 (2009)

- [22] S. Ahmed, T. Schuelke, Elsevier, *Diamond and Related Materials* 15, 389 (2006)
- [23] M. M. Wittebrood, D. H. Luijendijk, S. Stallinga, Th. Rasing, *Phys. Rev. E.*, 54 (5), 5232 (1996)
- [24] M. Marinelli, F. Mercuri, U. Zammit, F. Scudieri, *Phys. Rev. E.*, 58 (5), 5860 (1998)
- [25] [http://www.engineeringtoolbox.com/thermal-conductivity-d\\_429.html](http://www.engineeringtoolbox.com/thermal-conductivity-d_429.html)
- [26] <http://www.almazoptics.com/sapphire.htm> (thermal properties of sapphire)

# Appendix

## A. LabVIEW Instrument Control Code

Two separate LabVIEW codes were written to measure  $\kappa$  vs. T and  $\kappa$  vs. V. Several difficulties were encountered with file delimiter formatting mismatches between the Linux on which the LabVIEW program ran and the PC on which data analysis was performed. Ultimately, saving the data as excel workbooks solved most the problem, though a harmless warning would appear when the files were opened on a PC. Communication to the instruments was managed via VISA, which is a built-in library of functions used to communicate with GPIB, serial, VXI, and computer-based instruments. The code is written in a sequence structure, which ensures linear data flow between frames. The most important frames and the command sequences within them are outlined below. Details such as indicator lights are omitted.

### $\kappa$ vs. T measurement control:

#### Frame 1: Initialize and Configure

- Open VISA session
- Detect lock-in, temp controller, and multimeter with IDN\* queries
- Set lock-in settings: Output voltage and V measurement frequency (1000 Hz)
- Set PID parameters of temp controller: (P = 350, I = 50, D = 0)
- Configure multimeter for AC voltage measurement
- Set temp controller to starting temperature

#### Frame 2: FOR Loop (iterates with temperature step)

- step 1. Imbedded while loop runs until measured sample temperature is within tolerance (0.1 K) of set point
- step 2. Set lock-in time constant
- step 3. Set lock-in to 1<sup>st</sup> harmonic detection and set  $1\omega$  sensitivity → wait 120 s for temperature stabilization → measure sample temperature and V across heater
- step 4. Measure voltage across 5  $\Omega$  resistor → calculate current through sample and sample resistance
- step 5. Set lock-in to 3<sup>rd</sup> harmonic detection and set  $3\omega$  sensitivity → wait 20 s for  $3\omega$  signal stabilization
- step 6. Set fq range and run customized V $3\omega$  vs. fq sub VI → save data
- step 7. Repeat until data is taken at final temperature

#### Frame 3: Save and Cool

- Save  $V_{\text{heater}}$  vs. T,  $I_{\text{heater}}$  vs. T, and  $R_{\text{heater}}$  vs. T data
- Set temp controller to cool back to starting temperature

Frame 4: Close VISA session

### **$\kappa$ vs. V measurement control:**

Frame 1: Initialize and Configure

- Open VISA session
- Detect lock-in, electrometer, and multimeter with IDN\* queries
- Set lock-in settings: Output voltage and V measurement frequency (1000 Hz)
- Configure electrometer DCV operation
- Configure multimeter for AC voltage measurement

Frame 2: For Loop (iterates with voltage step)

- step 1. Set lock-in to 1<sup>st</sup> harmonic detection and set  $1\omega$  sensitivity → wait 10 s for signal stabilization → measure V across heater
- step 2. Measure voltage across 5  $\Omega$  resistor → calculate current through sample and sample resistance
- step 3. Set lock-in to 3<sup>rd</sup> harmonic detection and set  $3\omega$  sensitivity → wait 20 s for  $3\omega$  signal stabilization
- step 4. Set fq range and run customized V $3\omega$  vs. fq sub VI → save data
- step 5. Repeat until data is taken at final voltage

Frame 3: Save  $V_{\text{heater}}$  vs. V and  $R_{\text{heater}}$  vs. V data

Frame 4: Close VISA session

The excel files accumulated by LabVIEW are loaded into MATLAB<sup>®</sup> for analysis.

## **B. MATLAB code**

### **$\kappa$ vs. T analysis**

```
%% 10um Au-Ti Line Heater DATA ANALYSIS                               Mar 30, 2011
%% load Data (V3W vs FQ) at Multiple Temperatures
%X, Y, and fq
%variable notation: 1(line)-variable-EMPTY

%temperature: 310K - 331K
%cell thickness: empty cell
%Lock-in Vout: 2.0V (with 5ohm resistor in series)
```

```

%V1W at room temperature: 0.5V
%R at room temperature: ~19ohms
%heater length: 3.5mm
%fq range: 2Hz - 4.4kHz

%% EMPTY
Ntemp=63;%number of temperature steps

% RvsT
lRvsTEMPY=load('C:\Documents and Settings\socrates\My
Documents\CHTM\data\2011 files\AuTi
heaters\Mar30_40um_300to331K_EMPTY\RvsTEMPY.xls')
lREMPY=lRvsTEMPY(1:end,2)
lTEMPY=lRvsTEMPY(1:end,1)
plot(lTEMPY,lREMPY)
rfit=polyfit(lTEMPY(1:Ntemp),lREMPY(1:Ntemp),1)
lRval=polyval(rfit,lTEMPY(1:Ntemp))
plot(lTEMPY,lREMPY,'-o',lTEMPY(1:Ntemp),lRval)
lalphaEMPTYvec=rfit(1)./lREMPY
lalphaEMPTY=mean(lalphaEMPTYvec)%dR/dT/R usually .003

% calculate resistivity
resistivity=(300e-9)*(40e-6)*lREMPY/(3.5e-3)
plot(lTEMPY,resistivity,'-o',lTEMPY,(2.44e-
8)*ones(1,length(lTEMPY)), 'r',lTEMPY,(4.2e-7)*ones(1,length(lTEMPY)), 'r')
set(gca,'fontsize',14);xlabel('T (K)'); ylabel('\rho (\Omega-m)')
%resistivity of gold is 2.44e-8 ohm-m
%resistivity of Ti is 4.2e-7 ohm-m

% V1WvsT
lV1WvsTEMPY=load('C:\Documents and Settings\socrates\My
Documents\CHTM\data\2011 files\AuTi
heaters\Mar30_40um_300to331K_EMPTY\V1WvsTEMPY.xls')
lV1WEMPY=lV1WvsTEMPY(1:end,2)%peak
plot(lTEMPY,lV1WEMPY)
Vfit=polyfit(lTEMPY(1:Ntemp),lV1WEMPY(1:Ntemp),1)
lV1Wval=polyval(Vfit,lTEMPY(1:Ntemp))
plot(lTEMPY,lV1WEMPY,'-o',lTEMPY(1:Ntemp),lV1Wval)

% IvsT
lIvsTEMPY=load('C:\Documents and Settings\socrates\My
Documents\CHTM\data\2011 files\AuTi
heaters\Mar30_40um_300to331K_EMPTY\IvsTEMPY.xls')
lIEMPY=lIvsTEMPY(1:end,2)%peak
plot(lTEMPY,lIEMPY)

% V3WvsT
Nfq=15;
lXEMPY=zeros(Nfq,Ntemp);
lYEMPY=zeros(Nfq,Ntemp);
for ii=1:Ntemp

```

```

    str1=['load(''C:\Documents and Settings\socrates\My
Documents\CHTM\data\2011 files\AuTi
heaters\Mar30_40um_300to331K_EMPTY\V3WEMPTY_',int2str(ii),'.xls'')]
    LV3WvsfqEMPTY=eval(str1);
    LXEMPTY(1:end,ii)=LV3WvsfqEMPTY(1:Nfq,2);
    LYEMPTY(1:end,ii)=LV3WvsfqEMPTY(Nfq+1:end,2);
end
fqV=LV3WvsfqEMPTY(1:Nfq,1)
hold on
for ii=1:Ntemp
    plot(fqV,-
    LXEMPTY(1:end,ii),fqV,LYEMPTY(1:end,ii));xlabel('fq');ylabel('V3w')
end
hold off

% calculate dT for each fq sweep
ldTEMPY=zeros(Nfq,Ntemp);
for ii=1:Ntemp
    ldTEMPY(1:end,ii)=(-
    2*LXEMPTY(1:end,ii))/(LV1WEMPTY(ii)*lalphaEMPTYvec(ii));
end
% plot dT vs fq for each fq sweep
hold on
for ii=1:Ntemp
    plot(log(fqV(1:end)),ldTEMPY(1:end,ii),'-*')
    xlabel('fq'),ylabel('dT')
end
hold off
%%%%%%only first 10 points are in thin line regime

% calculate k (using V^2/R)
l=.0035;%heater length (m)
lPEMPTY=zeros(Ntemp,1);
lkEMPTYV=zeros(Ntemp,1);
for ii=1:Ntemp
    %calculate power per unit length at each temp
    lPEMPTY(ii)=(LV1WEMPTY(ii)^2)/(l*lREMPY(ii));
    %fit Re[dT] vs fq line at each temp
    lfitEMPTY=polyfit(log(fqV(1:10)),ldTEMPY(1:10,ii),1);
    %calculate k at each temp
    lkEMPTYV(ii)=lPEMPTY(ii)/(2*pi*abs(lfitEMPTY(1)));
end
plot(lTEMPY(1:Ntemp),lkEMPTYV,'o','linewidth',2);xlabel('T
(K)');ylabel('\kappa (W/m-K)')
set(gca,'fontsize',14)

% calculate k (using I^2R)
l=.0035;%heater length (m)
lPEMPTY=zeros(Ntemp,1);
lkEMPTYI=zeros(Ntemp,1);
for ii=1:Ntemp
    %calculate power per unit length at each temp
    lPEMPTY(ii)=(LIEMPTY(ii)^2)*lREMPY(ii)/l;
    %fit Re[dT] vs fq line at each temp
    lfitEMPTY=polyfit(log(fqV(1:10)),ldTEMPY(1:10,ii),1);
    %calculate k at each temp

```

```

    lkEMPTYI(ii)=lPEMPTY(ii)/(2*pi*abs(lfitEMPTY(1)));
end
plot(lTEMPY(1:Ntemp),lkEMPTYV,'o',lTEMPY(1:Ntemp),lkEMPTYI,'o','linewidth',
2)
set(gca,'fontsize',14);xlabel('T (K)');ylabel('\kappa (W/m-K)')

```

## **$\kappa$ vs. V analysis**

```

%% 20um Au-NiCr Line Heater DATA ANALYSIS          MAR 28, 2011
%% load Data (V3W vs FQ) at Multiple Function Generator frequencies
%X, Y, and fq

%temperature: 310K
%cell thickness: 80um MBBA
%Lock-in Vout: 1.5V
%R at room temperature: ~35ohms
%heater length: 3.5mm
%FG voltage amplitude: 19Vpp (square wave)

Nfgfq=10;% number of FG frequencies

%Resistance and V1w
V1WRdat=load('C:\Documents and Settings\socrates\My Documents\CHTM\data\2011
files\AuTi heaters\Mar28_310K_MBBA_FG_10mHzto10kHz\V1W&RvsFGfq_10V.xls');
Rvec=V1WRdat(1:Nfgfq,2)
V1Wvec=V1WRdat(Nfgfq+1:end,2);
FGfq=V1WRdat(1:Nfgfq,1);
plot(FGfq,Rvec)
plot(FGfq,V1Wvec)
%assume temperature coefficient is 0.0027/K
alph=0.0027;

%V3WvsfQ
Nfq=15;
X3Wmat=zeros(Nfq,Nfgfq);
Y3Wmat=zeros(Nfq,Nfgfq);

for ii=1:Nfgfq
    str1=['V3Wdat=load('C:\Documents and Settings\socrates\My
Documents\CHTM\data\2011 files\AuTi
heaters\Mar28_310K_MBBA_FG_10mHzto10kHz\V3W5CB_10V_',num2str(ii),'.xls')]
    eval(str1)
    X3Wmat(:,ii)=V3Wdat(1:Nfq,2);
    Y3Wmat(:,ii)=V3Wdat(Nfq+1:end,2);
end
fq=V3Wdat(1:Nfq,1);
%plot X3W and Y3W data
hold on
for ii=1:Nfgfq
    plot(fq,-X3Wmat(:,ii),'b')
    plot(fq,Y3Wmat(:,ii),'g')
end

```

```

xlabel('fq'),ylabel('X3\omega (blue), Y3\omega (green)')
hold off

%calculate dT for each fq sweep
dTmat=zeros(Nfq,Nfgfq)

for ii=1:Nfgfq
dTmat(:,ii)=(-2*X3Wmat(:,ii))/(V1Wvec(ii)*alph);
end
%plot dT vs fq for each fq sweep
hold on
for ii=1:Nfgfq
    plot(log(fq),dTmat(:,ii))
    xlabel('fq'),ylabel('dT')
end
hold off

%calculate k
l=.0035;%heater length (m)
kvec=zeros(1,Nfgfq);
Pvec=zeros(1,Nfgfq);

for ii=1:Nfgfq
    %calculate power per unit length at each temp
    Pvec(ii)=(V1Wvec(ii)^2)/(l*Rvec(ii));
    %fit Re[dT] vs fq line at each temp
    lfit=polyfit(log(2*pi*fq(1:10)),dTmat(1:10,ii),1);
    %calculate k at each temp
    kvec(ii)=Pvec(ii)/(2*pi*abs(lfit(1)));
    eval(str3)
end
semilogx(FGfq,kvec,'o','linewidth',3)
set(gca,'fontsize',12)
xlabel('FG fq (Hz)'),ylabel('\kappa W/m-K')

```